LU-TP 21-40
September 2021

Exploring a Two Higgs Doublet Model with a $U(1)$ Family Symmetry and a Complex Singlet

Michal Nowak

Department of Astronomy and Theoretical Physics, Lund University

Master thesis supervised by Roman Pasechnik,

and co-supervised by António P. Morais

LUND
UNIVERSITY

Abstract

In this project a two Higgs doublet model with a complex singlet and an extra family symmetry providing a mechanism for suppression of flavor changing neutral currents is explored. The goal is to investigate the phenomenological consistency of the model using a custom software framework. To this end, the scalar and Yukawa sectors of this extension of the Standard Model are explored in detail. The corresponding mass spectra, vacuum stability conditions and mixing matrices are presented. An inversion procedure, relating a subset of couplings to physical masses and mixing angles, for both the scalar and the quark Yukawa sector is implemented. In the search for phenomenologically viable parameter space regions, the Higgs alignment limit is relaxed while the Yukawa textures are allowed to take the most general complex values allowed by the symmetries. The phenomenological consistency of the model is investigated in the numerical analysis by comparing candidate points to experimental data from quark flavor violating processes and Higgs searches as well as vetoing any points that do not obey the limits set by electroweak precision observables. To facilitate the numerical analysis, a computer program utilizing several publicly available codes (SARAH, SPheno, HiggsBounds, HiggsSignals, flavio, FlavorKit) is constructed and run on a computer cluster. The results show that a symmetry-induced suppression of the flavor changing neutral currents takes place in the quark sector and the model survives the most stringent phenomenological constraints.

Populärvetenskaplig beskrivning

Den så kallade standardmodellen har länge betraktats som en av den moderna vetenskapens triumfer, tack vare dess oerhört exakta förutsägelser, som gång på gång har verifierats av experiment. Men från dess begynnelse har den alltid varit inkomplett: inte nog med att gravitationen, den kraft som vi människor är mest bekanta med, inte ens inkluderas i den så har olika, tidigare okända fenomen blivit upptäckta som standardmodellen inte kan förklara. Vidare, så finns det fenomen som trots att de ryms inom standardmodellen, inte kan förklaras på ett tillfredsställande sätt. Exempelvis finns det en mekanism för att generera kvarkarnas massor, men varför de olika kvarkarna har just de massor de har har ingen egentlig föklaring.

I jakt på nya teorier som kan både förklara fenomen som standardmodellen inte kan och samtidigt inte motsäga dess bekräftade förutsägelser, har olika utvidgningar av standardmodellen föreslagits. I den här uppsatsen utforskas en sådan utvidgning. I den, har standardmodellen berikats med extra Higgspartiklar vilka har en relativt stor potential att både kunna upptäckas inom snar framtid och att samtidigt förklara vissa av de mysterier som fortfarande plågar denna gren av fysiken. För att utröna om denna modell är värd att lägga ner mer tid på, har vi genomfört en datoranalys vars syfte har varit att undersöka om denna modell kan rymmas inom experimentellt etablerade gränsvärden. Datoranalyser av den här sorten består av enorma mängder ”gissande” av numeriska värden av modellens parametrar som, även för kraftfulla datorer, kan ta dagar om inte veckor. För att effektivisera denna procedur, har vi inom det här projektet tillämpat olika metoder vars syfte har varit att maximera antalet tidigt avvisade gissade värden på parametrarna. Resultaten visar på att det finns, i denna utvidgning av standardmodellen, parametervärden som både leder till intressant fysik och som inte strider mot experimentellt etablerade gränsvärden.

Contents

1 Introduction

The Standard Model (SM) of particle physics is the culmination of several decades of research in both theoretical and experimental physics. The discovery of the Higgs boson in 2012 [1, 2] confirmed the last major unverified element of the SM. It is a remarkable achievement of modern science, that can explain next to everything that we can perceive with our senses in the universe. Nevertheless, we know it to be seriously incomplete as a description of nature, as it for instance completely excludes gravity. In addition, astrophysical and cosmological observations have revealed that the problem of constructing a theory including both gravity and the SM is only the tip of the iceberg. According to those observations, hidden away from our perception are structures in the universe of vast magnitude that elude both our sight and our SM - the ominous dark matter and dark energy. Furthermore, there are subtle, known problems much closer to the SM that lack a first principle explanation as reflected in the following unanswered questions. What mechanism is responsible for the matter-antimatter asymmetry in the universe? What explains the hierarchical nature of the quark masses and mixing? Why do neutrinos have a mass? Why is it so small? The list goes on.

Efforts to answer such questions, as well as to put the SM into a greater context, have resulted in significant theoretical research output. Various theories, of larger and smaller scope, have been proposed to address the shortcomings of the SM. The more ambitious programs seek to cast the SM as an effective theory of a more holistic framework, which in the low energy limit reduces to the SM. This usually involves an enlargement of the SM gauge group to a much larger one that includes the SM interaction gauge groups as subgroups. Examples are the well-known grand unified theories (GUT), super-symmetric theories (SUSY) and of course string theories. Apart from the notorious mathematical difficulty these theories pose, an additional difficulty lies in the production of testable predictions. The energy scales at which the unique effects of these theories are expected to appear are thought to lie far beyond the technological capabilities of current and planned experimental facilities.

Other efforts at moving beyond the SM, take a different approach where instead of attempting to create unifying theories one minimally extends the SM. In this way, the predictions of the resulting model are much easier obtained. At the same time, the proposed extension of the SM is still expected to be a part of a GUT, only, one does not necessarily attempt to elucidate what that might be.

Examples of such minimal extensions of the SM are the scalar extensions. Among them, we have the multi-Higgs doublet models (or n-Higgs doublet models, nHDM for short), which for decades have played an important role in the attempts to expand the SM [3]. The nHDM extend the SM scalar sector by adding one or more Higgs doublets to the existing original doublet of the SM. Adding additional Higgs doublets to the SM is motivated by the fact that such models offer a rich collider phenomenology, additional sources of CP-violation, dark matter candidates, strong first order phase transitions etc. In particular, the CP-violation and first order phase transitions that accompany nHDM are interesting since the SM is unable to generate the observed baryon asymmetry of the universe [3].

A particular class of nHDM are the two Higgs doublet models (2HDM), in some sense the simplest nHDM. In them, the SM is extended by only one Higgs doublet. The first considerations of 2HDM were motivated by finding sources of CP-violation [4]. However, it was early noted that 2HDM, and nHDM in general, are plagued by a problem that does not appear in the SM scenario with one Higgs doublet. The added freedom introduced by the additional Higgs doublet allows for certain tree-level transitions between quark flavors that are heavily constrained by experiments. As a result, various schemes have been proposed over the years to mitigate this problem, often by invoking global symmetries [5, 6, 7]. In this thesis, we make use of one such mechanism.

A different kind of scalar extension is the inclusion of a scalar singlet into the Higgs sector. The singlets transform trivially under the SM gauge symmetries which prohibits their coupling to fermions and other SM particles. In addition, scalar singlets could have driven strong first order phase transitions in the early universe. Such a possibility is very interesting since it could help explaining the baryon-antibaryon asymmetry of the universe (the renowned Sakharov conditions for baryogenesis require strong out-of-equilibrium interactions [8]). Such strong first order phase transitions would have generated specific primordial gravitational wave spectra, that may be detectable by future gravitational wave observatories. All of this makes them very interesting as dark matter candidates.

This thesis builds upon a model that was proposed in [9], but not yet tested against phenomenological constraints. It includes a 2HDM SM extension with a complex singlet and a global $U(1)$ family symmetry. We perform a phenomenological analysis of the model suggested in [9]. To this end we develop a generic software tool that is publicly available [10].

This thesis is organized as follows. In section 2 we discuss physics that form the foundation of this thesis, in particular we introduce the Branco-Grimus-Lavoura (BGL) model [11] which plays an important role in the project. Next, in section 3 the scalar sector of the model is presented. The mass spectrum of the scalars is derived, inverted relations between physical parameters and couplings are introduced and the potential is examined. The next section, section 4, deals with the Yukawa sector. Here, we expand upon the discussion of the BGL-model. In section 5 we discuss various theoretical and experimental bounds that constrain the model and the numerical implementation of the parameter space scan. The results section, section 6, contains the plots summarizing the outcome of our scans. Conclusions are presented in section 7. In addition, in appendix A the mass matrices of the scalars are shown, appendix B contains a list of some parameters of the scalar sector expressed in terms of observables for use in numerical simulations and finally in appendix C we give a short manual of the software tool that was developed as a part of this project.

2 Background

In this section we outline some of the physics that is of crucial importance to this project. Firstly, we present a brief introduction to flavor physics. Measurements of flavor physics observables such as rare decays and oscillation amplitudes constitute an important test of the validity of any model aiming to extend beyond the SM. Next, a discussion of scalar extensions of the SM follows. As an important example of such extensions, the BGL-model is described.

2.1 Flavor physics

Considerations involving flavor physics have played an important role in the development of the SM of particle physics [12]. The flavor sector remains important in the continuing explorations of particle physics for a variety of reasons, including the large number of free parameters and sensitivity to new physics (NP) contributions.

The quark "flavors" (up-type: u,c,t and down-type: d,s,b), divided into three generations of increasing mass, have identical quantum numbers but differing masses. An explanation for the questions as to why such three copies exist and why the masses of those particle have the particular values they happen to have is still lacking.

The SM features a symmetry among the fermion flavors that, in the SM, is only broken by the Yukawa terms [12]. The quark fields are introduced into the SM Lagrangian in the *flavor* eigenstates as $SU(2)_L$ doublets and singlets:

$$Q_a = \begin{pmatrix} p_{L,a} \\ n_{L,a} \end{pmatrix}, \qquad p_{R,a},\ n_{R,a}, \qquad a = 1,2,3 \tag{2.1}$$

where p refer to up-type quark flavors (up, charm and top) while n refer to down-type quarks (down , strange and bottom). The index a runs over these three generations. The subscripts L, R refer to the chirality of the quark fields: due to the chirality-discriminating nature of the $SU(2)_L$ symmetry the right-chiral fields are always $SU(2)_L$ singlets while left-chiral fields are $SU(2)_L$ doublets.

In the SM, the fermion fields acquire mass though the Higgs mechanism via the Yukawa terms. Those belonging to quarks can be written as:

$$-\mathcal{L}_{\text{Yuk}} = \sum_{a,b} \left(\Gamma_{ab} \overline{Q}_a \Phi n_{R,b} + \Delta_{ab} \overline{Q}_a \tilde{\Phi} p_{R,b} + \text{h.c.} \right). \tag{2.2}$$

Φ is the SM Higgs doublet and its dual field is given by $\tilde{\Phi} = i\sigma_2 \Phi^\dagger$ where σ_2 is the second Pauli matrix

[1]. The Yukawa matrices Γ_{ab} and Δ_{ab} are *a priori* arbitrary and complex. In the SM, we can diagonalize the mass and Yukawa (interaction) matrices simultaneously since there is only one Higgs doublet present. The observable mass eigenstates are related to the flavor eigenstates through unitary transformations (flavor indices suppressed):

$$\begin{aligned} n_L &= U_L^d d_L, \quad & n_R &= U_R^d d_R, \\ p_L &= U_L^u u_L, \quad & p_R &= U_R^u u_R, \end{aligned} \tag{2.3}$$

where all the U matrices are unitary and 3×3, while the states d, u are the physical quark states (down and up type, respectively). Upon spontaneous symmetry breaking (s.s.b.) the Higgs field acquires a vacuum expectation value (vev), which can be rotated to the following position by a suitable gauge transformation:

$$\langle \Phi \rangle_0 = \frac{v}{\sqrt{2}} \begin{pmatrix} 0 \\ 1 \end{pmatrix} \tag{2.4}$$

where v is the value of the vev ≈ 246 GeV. The quark Yukawa terms now become the diagonal mass terms:

$$-\mathcal{L}_{\text{Yuk}} = \sum_{a,b} \left(m_{d,ab} \overline{d}_{L,a} d_{R,b} + m_{u,ab} \overline{u}_{L,a} u_{R,b} + \text{h.c.} \right), \tag{2.5}$$

where the diagonal mass matrices are given by:

$$m_{d,ab} = \text{diag}(m_d, m_s, m_b) = U_L^d \cdot \Gamma \cdot U_R^{d\dagger}, \tag{2.6}$$

where we introduced the down-type quark masses m_d, m_s, m_b. The situation is similar for up-type quarks.

Following this, one might ask: what physical effects do these unitary transformations of the quark fields have? They seem to have removed the problem of mixing flavors in the mass terms, but what about all the other parts of the SM Lagrangian?

It turns out [12, 14] that all the other terms of the Lagrangian are unaffected by such unitary transformations of the quark fields *except* for the terms describing the charged current ($J^{\mu+}$) interactions [2]. The flavor violation enters $J^{\mu+}$ via the CKM matrix V^{CKM}:

$$J^{\mu+} \propto \sum_a \overline{p}_{L,a} \gamma^\mu n_{L,a} = \sum_{a,b} \overline{u}_{L,a} \left[U_L^{u\dagger} U_L^d \right]_{ab} \gamma^\mu d_{L,b} = \sum_{a,b} \overline{u}_{L,a} V_{ab}^{CKM} \gamma^\mu d_{L,b}. \tag{2.7}$$

Where the flavor indices are written out to explicitly show the mixing. In what follows, we generally omit the flavor indices, but they are always implied.

Of particular interest is the fact that CP-violation is introduced to the quark sector via the CKM matrix. It is well known that a complex term in the Lagrangian violates the T (and therefore CP) symmetry. Since the CKM matrix is in general complex, the charged current terms may violate CP-symmetry. For this to happen however, it must *not* be possible to cancel out the complex phases of the CKM matrix by rephasing the quark fields (each quark field carries a redundant phase that can be suitably chosen to cancel out one phase from e.g. the CKM matrix). It turns out that at least three quark generations are needed to obtain a theory in which there is a complex phase in the CKM matrix that is physical (i.e. cannot be absorbed into the quark fields). The CKM matrix has been very successful in explaining the experimentally observed CP-violation in the quark sector. We return to the CKM matrix and its parametrization in section 4.2.

Since, as we have pointed out, the only flavor violation at tree level in the SM is confined to the charged current interactions, there are no tree-level *flavor changing neutral currents* (or FCNCs) in the SM. FCNSs do occur in the SM, but only via loops with internal $W^\pm$ bosons as is for example depicted in fig. 1. In addition, the FCNCs are further suppressed by the GIM mechanism [15], whereby all contributions at all orders in perturbation theory to the FCNC loop diagrams cancel by the unitarity of the CKM matrix if

[1] This ensures that the generation of up-type quark masses via the Yukawa terms respects $SU(2)_L$, see e.g. [13]

[2] For a pedagogical exposition of this fact and in particular why the neutral current interactions are flavor-diagonal in the SM see [12, 13, 14].

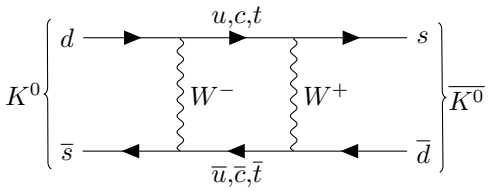

Figure 1: A diagram contributing to the flavor-violating mixing of the $K^0 - \overline{K^0}$ system [16].

they are independent of the quark masses. If the contributions depend on the quark masses, they come with differing signs and so there is a further cancellation of terms there. Of course, the SM quarks have wildly differing masses so some contributions survive, but the FCNCs processes in the SM are thus expected to be very suppressed as they are not only impossible at the tree-level, but also inhibited by both the smallness of the CKM matrix elements and the GIM mechanism.

FCNCs are naturally encountered and studied in certain meson systems, the neutral K, D and B mesons. As an example consider the neutral pseudoscalar kaon system: it is made up out of the two flavor eigenstates $|K^0\rangle = |d\overline{s}\rangle$ and $|\overline{K^0}\rangle = |s\overline{d}\rangle$ which mix at one loop level through e.g. the box diagram shown in fig. 1. Due to the aforementioned suppression mechanisms in the SM, these meson systems are very sensitive to BSM physics contributions. As we discuss in the next section, nHDM naturally feature tree-level FCNCs. Without fine-tuning or additional symmetries, these models typically predict FCNCs that are much too strong as compared to the experimental data, which favors models with FCNCs close to the weak SM ones. Therefore, any proposed nHDM must be carefully studied from the point of view of flavor violating observables such as neutral meson branching ratios, to make sure it complies with the stringent flavor physics limits.

2.2 Scalar extensions of the SM

The SM scalar sector, featuring a single Higgs doublet, is in a sense the minimal possible such sector. It suffices to explain the gauge boson masses and can accommodate for those of fermions. However, the gauge structure of the SM does not prohibit a more involved scalar sector [3]. It is therefore possible to extend the SM with additional scalar particles as long as the resulting model respects the (nowadays very stringent) bounds from experimental searches.

The motivation for such models comes from various considerations. Adding additional scalar particles produces a richer particle spectrum which can, in some models, contain dark matter candidate particles. The relative phases between the vev:s of the scalars can act as an additional source of CP-violation [4, 17]. The presence of additional scalar fields enriches the vacuum structure potentially enhancing the strength of FOPTs which, together with the CP-violation possibility, is relevant for the baryogenesis. In addition, the Yukawa sector becomes highly non-trivial with many possibilities for its modification emerging. A different type of motivation comes from unified theories such as supersymmetry, that naturally feature additional scalar particles.

While many possibilities for extending the scalar sector exist, here we will focus on some of the simpler ones. The archetypal such extensions feature additional Higgs $SU(2)_L$ doublets similar to the one already present in the SM. Such models, featuring n Higgs doublets, as commonly called n-Higgs doublet models (nHDM). The simplest case is of course the 2HDM which extends the SM scalar sector by one additional Higgs doublet. The introduction of additional scalar fields usually extends the scalar potential by many terms. Before discussing the 2HDM scalar potential, recall the SM scalar potential V_{SM}:

$$\mathcal{L}_{\text{SM}} \supset V_{\text{SM}} = \mu^2 |\Phi|^2 - \lambda |\Phi|^4 , \tag{2.8}$$

where $\mathcal{L}_{SM}$ denotes the SM Lagrangian and μ^2, λ are real parameters. Although there appears to be two degrees of freedom (d.o.f.) (μ^2 and λ), the minimization condition of the electroweak minimum reduces this to only one d.o.f., usually chosen to be λ (or the Higgs particle mass $m_h = v\sqrt{2\lambda}$).

The introduction of an additional Higgs doublet greatly extends the potential:

$$V_{\text{2HDM}} = \mu_1^2 \left|\Phi_1\right|^2 + \mu_2^2 \left|\Phi_2\right|^2 - \mu_3^2 \Phi_1^\dagger \Phi_2 - \left(\mu_3^2\right)^* \Phi_2^\dagger \Phi_1 + \lambda_1 \left|\Phi_1\right|^4 + \lambda_2 \left|\Phi_2\right|^4 + \lambda_3 \left|\Phi_1\right|^2 \left|\Phi_2\right|^2 + \\ + \lambda_4 \left(\Phi_1^\dagger \Phi_2\right)\left(\Phi_2^\dagger \Phi_1\right) + \left[\lambda_5 \left(\Phi_1^\dagger \Phi_2\right)^2 + \lambda_6 \left(\Phi_1^\dagger \Phi_1\right)\left(\Phi_1^\dagger \Phi_2\right) + \lambda_7 \left(\Phi_2^\dagger \Phi_2\right)\left(\Phi_1^\dagger \Phi_2\right) + \text{h.c.}\right], \tag{2.9}$$

here the parameters are also real except for μ_3^2, λ_5, λ_6 and λ_7 which can be complex.

The parameters in such a potential are not completely arbitrary however. The so-called tadpole conditions allow for the expression of one of them in terms of the others for each unique scalar multiplet (so two conditions in the 2HDM). We will return to the tadpole conditions when we discuss the scalar potential of our model in section 3. In addition, the parameters are restricted by the conditions of *boundedness from below* and the *unitarity*. The first refer to the physical requirement that the scalar potential must be bounded from below in all directions, so that it is not possible to reach states of arbitrarily low energy by moving in some direction in the field space. The second requirement concerns the constraint that the $2 \to 2$ scattering matrix must always be unitary. This can be violated in the high-energy regime if the quartic couplings have too large values [18]. We return to these conditions in section 5.1 where we apply them to our model.

Another type of scalar extensions that is of relevance here, is the scalar singlet extension. In contrast to the standard Higgs doublets, these extensions feature scalars which are gauge singlets and thus transform trivially under the SM symmetry transformations. By virtue of this, they have no tree-level couplings to any SM particles apart from other scalars. They can couple to e.g. the SM Higgs boson via the operator $\Phi^\dagger\Phi$ [3], which can produce potential terms such as $\propto \Phi^\dagger\Phi S^* S, \Phi^\dagger\Phi S, \Phi^\dagger\Phi S^*$. It is worth noting that the scalar singlet can be either real (1 d.o.f.) or complex (2 d.o.f.).

An often employed tool in the task of scalar model building and testing, is the usage of global symmetries to modify the structure of the theory. By imposing a continuous or discrete (or a combination thereof) global symmetry one can significantly simplify the model by e.g. forbidding various term in the potential and forcing certain Yukawa matrix elements to be zero. Such a procedure is often required when dealing with scalar extensions that go beyond the simple 2HDM and singlet models, as such models are often very complicated and an exhaustive investigation without simplifying assumptions is often prohibitively difficult. Furthermore, any general nHDM features tree-level FCNC. This follows from the fact that in such models all Higgs doublets couple to fermions via the Yukawa terms and hence the simultaneous diagonalization of mass and interaction matrices is impossible. In the next section we describe one approach at remedying this potentially problematic situation.

2.3 The Branco-Grimus-Lavoura Model

The BGL model [11], named after its inventors: G.C. Branco, W. Grimus and L. Lavoura, is one of the simplest and most important 2HDM. Its main feature is a "natural" way to suppress FCNCs. In this section, we aim to introduce the original BGL model and show how the FCNC suppression emerges at tree level. We will, following the original paper, focus on the Yukawa sector of the model. The scalar sector, along with the singlet extension of our model, will be discussed in section 3. Along the way, the techniques and expressions that we will introduce here will be used throughout the rest of this thesis.

The BGL model includes two Higgs $SU(2)_L$ doublets, Φ_j, $j = 1, 2$. The Yukawa Lagrangian is:

$$\mathcal{L}_Y = -\sum_{j=1}^{2} \left(\overline{Q}\Gamma_j \Phi_j n_R + \overline{Q}\Delta_j \tilde{\Phi}_j p_R\right) + \text{h.c.}, \tag{2.10}$$

here, the notation follows that of section 2.1. The difference is the summation over the Higgs doublets: there are now two Yukawa matrices for each quark type. For the most general form of such matrices, there will be strong tree-level FCNCs present. The special symmetry of the BGL model will remedy this situation, as we shall see.

Upon spontaneous symmetry breaking (s.s.b.) the Higgs fields acquire a vev, which can be rotated to the following position by a suitable gauge transformation:

$$\langle \Phi_j \rangle_0 = \frac{v_j e^{i\alpha_j}}{\sqrt{2}} \begin{pmatrix} 0 \\ 1 \end{pmatrix} \tag{2.11}$$

where v_j is the value of the vev of the jth Higgs doublet, α_j is a CP-breaking phase. The vev:s are related by $v = \sqrt{v_1^2 + v_2^2} \approx 246$ GeV the SM Higgs vev. Evaluating the terms in eq. (2.10) at this new electroweak minimum gives:

$$\begin{aligned} &\mathcal{L}_Y \overset{s.s.b}{\to} \frac{\bar{n}_L}{\sqrt{2}} \left(v_1 e^{i\alpha_1} \Gamma_1 + v_2 e^{i\alpha_2 \Gamma_2} \right) n_R + \frac{\bar{p}_L}{\sqrt{2}} \left(v_1 e^{-i\alpha_1} \Delta_1 + v_2 e^{-i\alpha_2} \Delta_2 \right) p_R + \text{h.c.} = \\ &= \bar{n}_L M_n n_R + \bar{p}_L M_p p_R + \text{h.c.} \end{aligned} \tag{2.12}$$

where we defined the mass matrices $M_{n,p}$ which are in general non-diagonal. They can be diagonalized by a unitary transformation to the mass basis eq. (2.3). The CKM matrix is given by, as before, $V^{CKM} = (U_L^u)^\dagger U_L^d$. This change of basis results in diagonal mass matrices:

$$D_d = (U_L^d)^\dagger M_n U_R^d, \qquad D_u = (U_L^u)^\dagger M_p U_R^u. \tag{2.13}$$

We can expand the scalar fields around the vev:s and parametrize them:

$$\Phi_j = \frac{e^{i\alpha_j}}{\sqrt{2}} \begin{pmatrix} \sqrt{2}\phi_j^+ \\ v_j + h_j + i\eta_j \end{pmatrix}, \tag{2.14}$$

where, ϕ_j^+ are a charged, complex scalar fields while the h_j and η_j are real fields [3].

In order to provide a natural way of suppressing the FCNCs, the BGL model features a global family symmetry, $\mathcal{S}$. Under this symmetry we have the following transformations:

$$Q_1 \to \omega Q_1, \qquad p_{R,1} \to \omega^2 p_{R,1}, \qquad \Phi_2 \to \omega \Phi_2. \tag{2.15}$$

Other fields transform under the identity transformation. For now, the only restrictions on the symmetry transformation ω are that $\omega \neq 1$, $\omega^2 \neq 1$ and $|\omega| = 1$. The requirement that all terms of the Lagrangian are to be invariant under the transformations in eq. (2.15) dictates the form of the Yukawa matrices Γ_j and Δ_j. It is straightforward to check that the allowed form of the Yukawa matrices is:

$$\begin{aligned} \Gamma_1 &= \begin{pmatrix} 0 & 0 & 0 \\ a_{21} & a_{22} & a_{23} \\ a_{31} & a_{32} & a_{33} \end{pmatrix}, \quad \Gamma_2 = \begin{pmatrix} b_{11} & b_{12} & b_{13} \\ 0 & 0 & 0 \\ 0 & 0 & 0 \end{pmatrix}, \\ \Delta_1 &= \begin{pmatrix} 0 & 0 & 0 \\ 0 & c_{22} & c_{23} \\ 0 & c_{32} & c_{33} \end{pmatrix}, \quad \Delta_2 = \begin{pmatrix} d_{11} & 0 & 0 \\ 0 & 0 & 0 \\ 0 & 0 & 0 \end{pmatrix}. \end{aligned} \tag{2.16}$$

We will give explanations for some of this structure. Regarding the first row of Γ_1, note that it couples $\overline{Q}_1$ to Φ_1 and n_R. But from the form of the transformations of eq. (2.15), we know that only $\overline{Q}_1$ transforms non-trivially under $\mathcal{S}$. Therefore, this row of Γ_1 must be zero to maintain the invariance of the Lagrangian under of $\mathcal{S}$. As a second example consider the d_{11} entry of Δ_2. It gives rise to the following term:

$$\overline{Q}_1 \cdot \tilde{\Phi}_2 \cdot d_{11} \cdot p_{R,1} \quad \overset{\text{symmetry trans.}}{\to} \quad \omega^* \overline{Q}_1 \cdot \omega^* \tilde{\Phi}_2 \cdot d_{11} \omega^2 \cdot p_{R,1} = |\omega|^4 \overline{Q}_1 \cdot \tilde{\Phi}_2 \cdot d_{11} \cdot p_{R,1} = \overline{Q}_1 \cdot \tilde{\Phi}_2 \cdot d_{11} \cdot p_{R,1}, \tag{2.17}$$

As we can see here, the effects of the symmetry transformation cancel, so the invariance under $\mathcal{S}$ is maintained and the matrix element d_{11} can remain arbitrary. The rest of the matrix elements can be similarly motivated.

[3] In the absence of a complex phase α_j they have definite transformation properties under CP-transformations : the h_j are CP-even while the η_j are CP-odd.

We note also, that due to the block-diagonal nature of the Δ matrices, the corresponding diagonalizing matrix U_L^u is also block-diagonal and in particular its first row and column is zero except for $(U_L^u)_{11}$ which can be chosen to be 1. Hence, we have the following relation for the topmost row of the CKM matrix:

$$(U_L^d)_{1i} = V_{1i}^{CKM} \equiv S_i. \tag{2.18}$$

Before we write out the Yukawa interactions of this model and evaluate the status of the FCNC in it, we introduce a convenient basis for the Higgs doublets that we will use repeatedly in this thesis. To motivate it, note that the eigenstates that we have used so far (belonging to the gauge, or Lagrangian, basis) are not necessarily the same as the mass eigenstates or as the states that couple to the weak vector bosons [4]. In particular in 2HDMs, we have two real scalars that are CP-even if the phase α_j vanishes, h_1 and h_2, but experimental data suggests that the weak vector bosons couple to only one such scalar, H^0. This observation suggests a new basis, where the state that couples to the vector bosons is a linear combination of the gauge eigenstates h_1 and h_2. This is the so called Higgs basis, a basis in the space of Higgs doublets obtained by performing an orthogonal rotation such that one combination of the Higgs doublets gets the entire vev. This way, the massless Goldstone modes are made explicit and can be discarded from the considerations of Yukawa couplings. However, this choice of basis is not physical (it is not the same as the physical mass basis) but rather a convenient device for exploring the model.

To recover a SM-like Higgs particle we need a candidate particle in our model that has the same (or very similar) couplings to the weak vector bosons. These couplings appear in the covariant derivative terms of the Lagrangian $|\mathcal{D}^\mu \Phi_a|^2$. Following [19] it is easy to show that the coupling of the CP-even components of the Higgs doublets to the charged weak vector bosons is:

$$|\mathcal{D}^\mu \Phi_a|^2 \ni \frac{g^2}{2} W_\mu^+ W^{\mu-} \sum_{a=1}^{2} v_a h_a = \frac{g^2 v}{2} W_\mu^+ W^{\mu-} \left(\frac{1}{v} \sum_{a=1}^{2} v_a h_a \right), \tag{2.19}$$

what this shows is that we can have the a SM-like Higgs boson if we identify it with the linear combination $H^0 = \left(\frac{1}{v} \sum_{a=1}^{2} v_a h_a \right)$ and if the vev present here is equal to the electroweak symmetry breaking scale: $v = 246$ GeV.

The above observation suggests a new basis of states [19], [20], [21]. We have so far worked in the gauge (or Lagrangian) basis. The above identification of the H^0 combination of gauge eigenstates as the SM-like Higgs boson with correct coupling to the gauge bosons implies that it is a state in the Higgs basis. The rotation that takes the Higgs fields to this basis is, explicitly:

$$\begin{cases} v_1 = v \cos\beta \\ v_2 = v \sin\beta \end{cases} \quad \text{with:} \quad \tan\beta = \frac{v_2}{v_1}, \; v = \sqrt{v_1^2 + v_2^2}, \quad \text{so that:} \quad \begin{pmatrix} H^0 \\ R \end{pmatrix} = \begin{pmatrix} \cos\beta & \sin\beta \\ -\sin\beta & \cos\beta \end{pmatrix} \begin{pmatrix} h_1 \\ h_2 \end{pmatrix}, \tag{2.20}$$

where R is the orthogonal combination of H^0. The change of basis is thus accomplished by:

$$O = \frac{1}{v} \begin{pmatrix} v_1 & v_2 \\ v_2 & -v_1 \end{pmatrix} = \begin{pmatrix} \cos\beta & \sin\beta \\ -\sin\beta & \cos\beta \end{pmatrix}, \; \rightarrow \; \begin{pmatrix} H^0 \\ R \end{pmatrix} = O \begin{pmatrix} h_1 \\ h_2 \end{pmatrix}, \; \begin{pmatrix} G^0 \\ I \end{pmatrix} = O \begin{pmatrix} \eta_1 \\ \eta_2 \end{pmatrix}, \; \begin{pmatrix} G^+ \\ H^+ \end{pmatrix} = O \begin{pmatrix} \phi_1^+ \\ \phi_2^+ \end{pmatrix}, \tag{2.21}$$

where we have the three Goldstone modes G^0, G^+ and $G^- = (G^+)^\dagger$ that according to the theory of electroweak interactions become the longitudinal polarization states of the Z^0, W^+ and W^- bosons. We will elaborate on the properties of the other combinations in section 3.3, for now note that they are pairwise orthogonal since the matrix $O \in \mathsf{SO}(2)$.

We are now in position to evaluate the couplings of the scalars to the quarks. The procedure is to start with eq. (2.10), insert the Higgs doublets parametrized as in eq. (2.14), diagonalize the states with the

[4] The distinction between the mass and (implicitly) gauge basis was made on the previous page for quarks (i.e. p, n vs u, d). Now we are proposing a similar but distinct change for the Higgs doublets.

matrices eq. (2.3) and use the Higgs basis. The Δ_j terms:

$$\begin{aligned}
&-\sum_{j=1}^{2}\left(\bar{Q}\Delta_j\tilde{\Phi}_j p_R+\text{h.c.}\right)\overset{\text{s.s.b.}}{\to}-i\sum_{j=1}^{2}e^{-i\alpha_j}\bar{Q}\Delta_j\sigma_2\begin{pmatrix}\phi_j^-\\ \frac{1}{\sqrt{2}}(h_j-i\eta_j)\end{pmatrix}p_R+\text{h.c.}=\\
&=-\frac{H^0\bar{u}_L}{v}D_u u_R-\frac{R\bar{u}_L}{v}N_u u_R+i\frac{I\bar{u}_L}{v}N_u u_R+\frac{H^-\bar{d}_L\sqrt{2}}{v}\left(V^{CKM}\right)^\dagger N_u u_R+\text{h.c.}.
\end{aligned}\tag{2.22}$$

Where $N_u=\frac{v_2}{v_1}\text{diag}(0,m_{u2},m_{u3})-\frac{v_1}{v_2}\text{diag}(m_{u1},0,0)$. It is evident that there are no FCNCs in this part of the Yukawa sector.

Let us now proceed to the Γ_j terms. We can proceed here just like we did for the Δ_j terms, however the matrix corresponding to N_u, which we denote by N_d, will not be diagonal. In particular, what we could do in eq. (2.22) was to utilize the block-diagonal form of the Δ matrices to perform a simultaneous diagonalization: the matrices $\Delta'_j=(U_L^u)^\dagger\Delta_j U_R^u$ are block diagonal. This cannot be done for the Γ_j matrices: $\Gamma'_j=(U_L^d)^\dagger\Gamma_j U_R^d$ are not block diagonal. Instead, we manipulate the corresponding terms into a useful form:

$$\begin{aligned}
&\frac{1}{\sqrt{2}}\left(v_2e^{-i\alpha_1}\Gamma'_1-v_1e^{-i\alpha_2}\Gamma'_2\right)=\frac{1}{\sqrt{2}}\left(\frac{v_2}{v_1}v_1e^{-i\alpha_1}\Gamma'_1+\frac{v_2}{v_1}v_2e^{-i\alpha_2}\Gamma'_2-\frac{v_2}{v_1}v_2e^{-i\alpha_2}\Gamma'_2-v_1e^{-i\alpha_2}\Gamma'_2\right)=\\
&=\frac{v_2}{v_1}D_d-\left(\frac{v_2}{v_1}+\frac{v_1}{v_2}\right)\frac{v_2e^{-i\alpha_2}\Gamma'_2}{\sqrt{2}}
\end{aligned}\tag{2.23}$$

Here, we have managed to isolate the non-diagonal, FCNC inducing part to the second term. Now, recall the explicit form of the two Γ_j matrices, eq. (2.16). We can introduce the projection operator:

$$P=\begin{pmatrix}1&0&0\\0&0&0\\0&0&0\end{pmatrix},\quad\to\quad\frac{v_2e^{i\alpha_2}\Gamma_2}{\sqrt{2}}=PM_d\tag{2.24}$$

to rewrite the last term of eq. (2.23):

$$\frac{v_2e^{i\alpha_2}\Gamma'_2}{\sqrt{2}}=\left(U_L^d\right)^\dagger PM_dU_R^d=\left(U_L^d\right)^\dagger PU_L^d\left(U_L^d\right)^\dagger M_dU_R^d=S_j^\dagger S_iD_d,\tag{2.25}$$

where we used that $PU_L^d=\left(U_L^d\right)_{1i}=S_i$. With this, we can rewrite the expression eq. (2.23) into:

$$\frac{v_2}{v_1}D_d-\left(\frac{v_2}{v_1}+\frac{v_1}{v_2}\right)\frac{v_2e^{-i\alpha_2}\Gamma'_2}{\sqrt{2}}=\frac{v_2}{v_1}D_d-\left(\frac{v_2}{v_1}+\frac{v_1}{v_2}\right)S_j^\dagger S_iD_d\equiv N_d\tag{2.26}$$

and the other part of the Yukawa Lagrangian for quarks is:

$$\begin{aligned}
&-\sum_{j=1}^{2}\left(\overline{Q}\Gamma_j\Phi_jn_R+\text{h.c.}\right)\overset{\text{s.s.b.}}{\to}\\
&-\frac{H^0\bar{d}_L}{v}D_dd_R+\frac{R\bar{d}_L}{v}N_dd_R+i\frac{I\bar{d}_L}{v}N_dd_R+\frac{H^+\bar{u}_L\sqrt{2}}{v}V^{CKM}N_dd_R+\text{h.c.}.
\end{aligned}\tag{2.27}$$

The two equations eq. (2.22) and eq. (2.27) comprise the quark Yukawa sector of the BGL model. Using the definition of N_d, eq. (2.26), it is easy to see where all the (tree-level) FCNC are coming from: the coupling of the down-type quarks to the scalars R and I in eq. (2.27). They are, by virtue of the form of N_d, controlled by the elements of the CKM matrix.

3 The Scalar Sector

In this section we introduce the model that this thesis explores. We then elaborate on its scalar sector by deriving the tadpole conditions, its mass spectrum and by discussing how it can be sampled by a computer program using the so-called inversion procedure. The investigation of the Yukawa sector is deferred to section 4.

3.1 The model

The model considered here was introduced in the following Ph.D. thesis by Astrid Ordell as "νBGL-1": [9]. The Lagrangian is invariant under $SU(3)_C \times SU(2)_L \times U(1)_Y \times U(1)_F$, where the first three symmetries are the SM ones and $U(1)_F$ is a new global family symmetry, acting on quarks, leptons and scalars (cf. the BGL-model discussed in section 2.3). The model extends the SM scalar sector to include two Higgs doublets Φ_a, $a = 1, 2$ and a complex scalar singlet $\mathcal{S}$, all of which can have potentially different $U(1)_F$ charges. The potential contains terms that softly break the $U(1)_F$ symmetry, giving rise to a massive pseudo-Goldstone boson. The family-symmetry charge assignments in the νBGL-1 model are presented in table 1.

Table 1: *Table of the charges under $U(1)_F$ of the νBGL-1 model. The rows specify the components of the flavor-multiplets (Q, u_R etc.). Of course, not all multiplets have the same number of components, hence the missing entries. The parameters x and y can be any rational numbers, as long as they are chosen consistently throughout the implementation.*

Component	Q	u_R	d_R	L	e_R	N_R	Φ	$\mathcal{S}$
1	x	y	$2x-y$	$-3x$	$-2x-y$	$-4x+y$	$-x+y$	$8x-2y$
2	x	y	$2x-y$	$-3x$	$-2y-y$	$-4x+y$	$-9x+3y$	-
3	$-7x+2y$	$-16x+5y$	$2x-y$	$21x-6y$	$30x-9y$	$12x-3y$	-	-

The $SU(2)_L \times U(1)_Y$ representations under which the scalars transform are:

$$\Phi_1 = (\mathbf{2}, 1) \qquad \Phi_2 = (\mathbf{2}, 1) \qquad \mathcal{S} = (\mathbf{1}, 0)\,. \tag{3.28}$$

Throughout this project, we assume a CP-conserving scalar sector. The complex phase of the vev is therefore set to zero and all couplings of the scalar potential are assumed to be real. In any future extensions of this project, this assumption could certainly be relaxed and new phenomena could be investigated. In addition, in this thesis we implement a slightly simplified version of the νBGL-1 model, namely we exclude the right-handed sterile neutrinos N_R and keep only the massless, left-handed SM neutrinos. As a consequence, the lepton sector features no tree-level FCNCs.

3.2 The scalar potential

The information from the previous section allows us to write down the scalar potential:

$$\begin{aligned} V_0 = {} & \mu_1^2 |\Phi_1|^2 + \mu_2^2 |\Phi_2|^2 + \lambda_1 |\Phi_1|^4 + \lambda_2 |\Phi_2|^4 + \lambda_3 |\Phi_1|^2 |\Phi_2|^2 + \lambda_4 \left(\Phi_1^\dagger \Phi_2\right)\left(\Phi_2^\dagger \Phi_1\right) + \\ & + \mu' |\mathcal{S}|^2 + \lambda_1' |\mathcal{S}|^4 + \lambda_2' |\Phi_1|^2 |\mathcal{S}|^2 + \lambda_3' |\Phi_2|^2 |\mathcal{S}|^2 + \left(\mu_3^2 \Phi_2^\dagger \Phi_1 + \text{h.c.}\right) + \left(\frac{1}{2}\mu_b^2 \mathcal{S}^2 + \text{h.c.}\right). \end{aligned} \tag{3.29}$$

Clearly, all of the above terms are invariant under the four symmetry groups separately except for the last two terms. The Higgs doublets transform in the same way under $SU(2)_L$ while the $\mathcal{S}$ is a singlet so all the above terms are invariant under $SU(2)_L$. The same applies to $U(1)_Y$, upon inspection of eq. (3.28). The last two terms are the "soft-breaking terms"[5] that break the global $U(1)_F$ symmetry.

In addition to these terms, we can write down phase-dependent terms, i.e. terms that depend on the relative charges $U(1)_F$ of the Higgs doublets and the singlet scalar [22, 23]. These are:

$$V_1 = \begin{cases} a_1 \Phi_1^\dagger \Phi_2 \mathcal{S} + \text{h.c.} & \text{, or} \\ a_2 \Phi_1^\dagger \Phi_2 \mathcal{S}^* + \text{h.c.} & \text{, or} \\ a_3 \Phi_1^\dagger \Phi_2 \mathcal{S}^2 + \text{h.c.} & \text{, or} \\ a_4 \Phi_1^\dagger \Phi_2 (\mathcal{S}^*)^2 + \text{h.c.} \end{cases} \tag{3.30}$$

[5]Soft-breaking terms are terms in the Lagrangian that break a symmetry, but in a way that does not spoil the high-energy behavior of the theory.

To demonstrate the phase dependence, we show the $U(1)_F$ transformation for the first term:

$$a_1\Phi_1^\dagger\Phi_2\mathcal{S} \;\;\rightarrow\;\; a_1\cdot e^{-i\alpha\chi_1}\Phi_1^\dagger\cdot e^{i\alpha\chi_2}\Phi_2\cdot e^{i\alpha\chi_\mathcal{S}}\mathcal{S} = e^{i\alpha(\chi_2-\chi_1+\chi_\mathcal{S})}\cdot a_1\Phi_1^\dagger\Phi_2\mathcal{S} \tag{3.31}$$

clearly, this term is only invariant under the family symmetry if $\chi_\mathcal{S} = \chi_1 - \chi_2$. A similar analysis shows that the corresponding valid choices for the charges of the terms in eq. (3.30) are:

$$\begin{aligned} a_1\Phi_1^\dagger\Phi_2\mathcal{S} + \text{h.c.} \;&\rightarrow\; \chi_\mathcal{S} = \chi_1 - \chi_2 \\ a_2\Phi_1^\dagger\Phi_2\mathcal{S}^* + \text{h.c.} \;&\rightarrow\; \chi_\mathcal{S} = \chi_2 - \chi_1 \\ a_3\Phi_1^\dagger\Phi_2\mathcal{S}^2 + \text{h.c.} \;&\rightarrow\; \chi_\mathcal{S} = \frac{1}{2}(\chi_1 - \chi_2) \\ a_4\Phi_1^\dagger\Phi_2(\mathcal{S}^*)^2 + \text{h.c.} \;&\rightarrow\; \chi_\mathcal{S} = \frac{1}{2}(\chi_2 - \chi_1)\,. \end{aligned} \tag{3.32}$$

Note that only one of the terms in eq. (3.30) can be present in the Lagrangian at the same time if it is to respect the family symmetry. In the νBGL-1 model only the a_1 term can be present (substitute values from table 1 into the χ:s to verify)[6]. Although we will carry out all the subsequent analysis with all four terms present for future reference, it is to be understood however that in obtaining our results we have set all the coefficients except a_1 to zero.

The next step is to obtain the minimum of the potential around which we will then expand the fields. Firstly, the s.s.b. causes vev to appear. As explained at the start of this section, we work in the CP-conserving case, so all parameters are real and the vev:s will be real:

$$\langle\Phi_a\rangle = \frac{v_a}{\sqrt{2}}\begin{pmatrix}0\\1\end{pmatrix} \qquad \langle\mathcal{S}\rangle = \frac{v_s}{\sqrt{2}} \tag{3.33}$$

We now require that the potential minimum is in fact at the vev by evaluating the derivatives of the fields at the vev and setting them equal to zero. These "tadpole" equations are thus:

$$\left\langle\frac{\partial V}{\partial\Phi_a}\right\rangle\Big|_{\Phi_a=\langle\Phi_a\rangle} = 0 \tag{3.34}$$

The scalar fields can be expanded around the vev's. We choose the parametrization employed in eq. (2.14) alongside the following parametrization of the scalar singlet:

$$\mathcal{S} = \frac{1}{\sqrt{2}}(v_s + \sigma + i\rho) \tag{3.35}$$

where σ and ρ are real fields. The derivative w.r.t. Φ_1:

$$\frac{\partial V}{\partial\Phi_1} = \mu_1^2\Phi_1^\dagger + 2\lambda_1\Phi_1^\dagger\Phi_1\Phi_1^\dagger + \lambda_3\Phi_1^\dagger\Phi_2^\dagger\Phi_2 + \lambda_4\Phi_1^\dagger\Phi_2\Phi_2^\dagger + \lambda_2'\Phi_1^\dagger\mathcal{S}^\dagger\mathcal{S} + a_1\Phi_2^\dagger\mathcal{S}^* + a_2\Phi_2^\dagger\mathcal{S} + a_3\Phi_2^\dagger\mathcal{S}^{*2} + a_4\Phi_2^\dagger\mathcal{S}^2 + \mu_3^2\Phi_2^\dagger \tag{3.36}$$

where it is understood, that only one of the a_i terms can be non-zero as explained above. Similarly, for Φ_2:

$$\frac{\partial V}{\partial\Phi_2} = \mu_2^2\Phi_2^\dagger + 2\lambda_2\Phi_2^\dagger\Phi_2\Phi_2^\dagger + \lambda_3\Phi_1^\dagger\Phi_1\Phi_2^\dagger + \lambda_4\Phi_1^\dagger\Phi_2^\dagger\Phi_1 + \lambda_3'\Phi_2^\dagger\mathcal{S}^\dagger\mathcal{S} + a_1\Phi_1^\dagger\mathcal{S} + a_2\Phi_1^\dagger\mathcal{S}^* + a_3\Phi_1^\dagger\mathcal{S}^2 + a_4\Phi_1^\dagger\mathcal{S}^{*2} + \mu_3^2\Phi_1^\dagger. \tag{3.37}$$

[6]Technically we could allow for the other terms as well, requiring for instance small couplings. In this way we would have additional sources of soft breaking of the family symmetry. Including the dimension four terms (a_3 and a_4) however would affect both vacuum stability and tree-level unitarity of the scattering matrix in a non-trivial way, hence we do not consider them in this project. Although the same argument does not apply to the other trilinear term a_2 (since it has a lower dimension in the fields, the presence of quartic terms in the scalar potential makes it irrelevant in the high-energy limit), we set it also to zero for simplicity.

We would now like to proceed as indicated in eq. (3.34) by evaluating the above two derivatives at the vev. Normally (i.e. in the SM Higgs mechanism), we would factor out the doublet in eq. (3.34) and set the resulting sum equal to zero. But a quick inspection of eq. (3.36) and eq. (3.37) convinces us that this is impossible, since the phase-dependent potential terms depend upon a different doublet than the rest of the terms. So we cannot factor out anything. However, guided by [23] we recognize that the two equations eq. (3.36), eq. (3.37) combine into a matrix equation.

To see this, consider the following. The terms in eq. (3.29) and eq. (3.30) can be seen as a matrix left-multiplied by a hermitian conjugated doublet and right-multiplied by a doublet i.e $\Phi_a^\dagger \mathcal{M}_{ab} \Phi_b$. For example:

$$\begin{aligned} \mu_1^2 \Phi_1^\dagger \Phi_1 &\rightarrow \Phi_1^\dagger \cdot \mu_1^2 \cdot \Phi_1 \\ \lambda_1 \left(\Phi_1^\dagger \Phi_1\right)^2 &\rightarrow \Phi_1^\dagger \cdot \lambda_1 \left(\Phi_1^\dagger \Phi_1\right) \cdot \Phi_1 \\ \lambda_4 \left(\Phi_1^\dagger \Phi_2\right)\left(\Phi_2^\dagger \Phi_1\right) &\rightarrow \frac{1}{2}\Phi_1^\dagger \cdot \lambda_4 \left(\Phi_2^\dagger \Phi_1\right) \cdot \Phi_2 + \frac{1}{2}\Phi_2^\dagger \cdot \lambda_4 \left(\Phi_1^\dagger \Phi_2\right) \cdot \Phi_1 \end{aligned} \tag{3.38}$$

where the terms on the right-hand side can interpreted as matrix elements sandwiched between doublets, with the index being the Higgs-doublet label 1,2. We can view the derivative in eq. (3.36), eq. (3.37) as removing one of the outer doublets. Hence the terms in eq. (3.36), eq. (3.37) can be viewed as matrix elements times the remaining doublet. Proceeding as in eq. (3.38), we can group the terms in eq. (3.36) accordingly:

$$\frac{\partial V}{\partial \Phi_1} = \Phi_1^\dagger \left(\mu_1^2 + 2\lambda_1 \Phi_1 \Phi_1^\dagger + \lambda_3 \Phi_2^\dagger \Phi_2 + \lambda_2' \mathcal{S}^\dagger \mathcal{S}\right) + \Phi_2^\dagger \left(\lambda_4 \Phi_1^\dagger \Phi_2 + a_1 \mathcal{S}^* + a_2 \mathcal{S} + a_3 \mathcal{S}^{*2} + a_4 \mathcal{S}^2 + \mu_3^2\right). \tag{3.39}$$

Using the form: $\Phi_a^\dagger \mathcal{M}_{ab}^2 \Phi_b$ we see that the first term in the above equation is $\Phi_1^\dagger \mathcal{M}_{11}^2$ and the second one is $\Phi_2^\dagger \mathcal{M}_{21}^2$. We can proceed with eq. (3.37) analogously. What we really are interested in however, is the expectation value of this (c.f. eq. (3.34)). We therefore evaluate eq. (3.39) at the vev and collect the terms:

$$\begin{aligned} \mathcal{M}_{11}^2 &= \mu_1^2 + \lambda_1 v_1^2 + \frac{1}{2}\lambda_3 v_2^2 + \frac{1}{2}\lambda_2' v_s^2 \qquad \mathcal{M}_{22}^2 = \mu_2^2 + \lambda_2 v_2^2 + \frac{1}{2}\lambda_3 v_1^2 + \frac{1}{2}\lambda_3' v_s^2 \\ \mathcal{M}_{12}^2 &= \mathcal{M}_{21}^2 = \frac{1}{2}\lambda_4 v_1 v_2 + \frac{1}{\sqrt{2}} a_1 v_s + \frac{1}{\sqrt{2}} a_2 v_s + \frac{1}{2} a_3 v_s^2 + \frac{1}{2} a_4 v_s^2 + \mu_3^2. \end{aligned} \tag{3.40}$$

The tadpole equations for the Higgs fields are thus equivalent to:

$$\mathcal{M}_{ab}^2 v_b = 0. \tag{3.41}$$

We have still not considered the final tadpole equation:

$$\left\langle \frac{\partial V}{\partial \mathcal{S}} \right\rangle \Big|_{\mathcal{S}=\langle \mathcal{S} \rangle} = 0. \tag{3.42}$$

Proceeding as before:

$$\frac{\partial V}{\partial \mathcal{S}} = \mu'^2 \mathcal{S}^\dagger + \mu_b^2 \mathcal{S} + 2\lambda_1' \mathcal{S}^\dagger \mathcal{S} \mathcal{S}^\dagger + \lambda_2' \Phi_1^\dagger \Phi_1 \mathcal{S}^\dagger + \lambda_3' \Phi_2^\dagger \Phi_2 \mathcal{S}^\dagger + a_1 \Phi_1^\dagger \Phi_2 + a_2 \Phi_2^\dagger \Phi_1 + 2a_3 \Phi_1^\dagger \Phi_2 \mathcal{S} + 2a_4 \Phi_2^\dagger \Phi_1 \mathcal{S}, \tag{3.43}$$

then evaluating this at the vev and setting it equal to zero gives the tadpole equation:

$$0 = v_s \left(\mu'^2 + \mu_b^2 v_s + \lambda_1' v_s^2 + \frac{1}{2}\left(\lambda_2' v_1^2 + \lambda_3' v_2^2\right)\right) + \frac{v_1 v_2}{\sqrt{2}}\left(a_1 + a_2\right) + v_s v_1 v_2 \left(a_3 + a_4\right) \tag{3.44}$$

For future convenience we want to solve the tadpole equations for μ_1^2, μ_2^2, μ'^2 as functions of the λ:s and vev:s. This can readily be done:

$$\begin{aligned}
\mu_1^2 &= -\frac{\sqrt{2}a_1 v_2 v_s + \sqrt{2}a_2 v_2 v_s + a_3 v_2 v_s^2 + a_4 v_2 v_s^2 + 2\lambda_1 v_1^3 + \lambda_3 v_1 v_2^2 + \lambda_4 v_1 v_2^2 + \lambda_2' v_1 v_s^2 + 2 v_2 \mu_3^2}{2 v_1}, \\
\mu_2^2 &= -\frac{\sqrt{2}a_1 v_1 v_s + \sqrt{2}a_2 v_1 v_s + a_3 v_1 v_s^2 + a_4 v_1 v_s^2 + \lambda_3 v_1^2 v_2 + \lambda_4 v_1^2 v_2 + 2\lambda_2 v_2^3 + \lambda_3' v_2 v_s^2 + 2 v_1 \mu_3^2}{2 v_2}, \\
\mu'^2 &= -\frac{\sqrt{2}a_1 v_1 v_2 + \sqrt{2}a_2 v_1 v_2 + 2a_3 v_1 v_2 v_s + 2a_4 v_1 v_2 v_s + \lambda_2' v_1^2 v_s + \lambda_3' v_2^2 v_s + 2\lambda_1' v_s^3 + 2\mu_b^2 v_s}{2 v_s}.
\end{aligned} \tag{3.45}$$

3.3 The scalar mass spectrum

In this section we investigate the mass spectrum of the scalar sector. As a consequence of the Nambu-Goldstone theorem, the s.s.b. causes three massless Goldstone bosons to emerge, which, due to the Glashow-Weinberg-Salam theory and the underlying Higgs mechanism, become the longitudinal polarization states of the weak vector bosons, thereby giving them mass.

Furthermore, the same mechanism would cause a massless Goldstone boson to emerge in the complex singlet since it also acquires a non-zero vev. However, the presence of the soft-breaking terms spoils the $U(1)_F$ symmetry. The resulting boson is thus pseudo-Goldstone i.e. it has a non-zero mass that can in principle have any value.

In addition to observing all of the above predictions appear in our model, we want to recover the newly discovered Higgs boson [1, 2] in our model despite the fact that we now have two Higgs doublets and a singlet that can mix.

First, consider this last objective. To recover a SM-like Higgs particle we need a candidate particle in our model that has the same (or very similar) couplings to the weak vector bosons. Recall that we have already mentioned this in the section 2.3 when we discussed the Higgs basis: it is possible to perform an orthogonal rotation to a basis where one of the states has the correct couplings. Note that the complex singlet does not enter into these considerations since the couplings appear in the covariant derivative terms of the Lagrangian $|\mathcal{D}^\mu \Phi_a|^2$ thus the complex singlet cannot couple to the electroweak vector bosons (apart from through the Higgs bosons after EWSB) since it does not transform under their symmetry groups, c.f. eq. (3.28).

What we did not mention in section 2.3 however is the fact that the physical mass eigenstates need not be the same as the gauge or interaction eigenstates: in fact they can be any orthogonal combination of the Higgs basis eigenstates. Since we know experimentally that the detected Higgs boson (mass eigenstate) has up to considerable precision, the expected couplings to the gauge bosons, this needs to be taken into consideration when evaluating a model's phenomenological validity.

The limit in which the mass and Higgs basis eigenstates coincide is called the Higgs alignment limit. In what follows, we first investigate the Higgs and mass bases of our model before exploring the Higgs alignment condition.

The treatment of mass and Higgs bases is conveniently done by considering the real and imaginary fields as components of a vector space. The neutral scalar fields are customarily decomposed into real fields (in our CP-conserving case, CP-even and -odd fields) while the charged scalars are not decomposed, as shown in eq. (2.14) and eq. (3.35). We thus have the following two vectors of states:

$$\boldsymbol{\varphi} = (h_1, h_2, \sigma, \eta_1, \eta_2, \rho)^T \qquad \boldsymbol{\phi} = \left(\phi_1^+, \phi_2^+\right)^T. \tag{3.46}$$

The real scalars can be grouped into two sets depending on their transformation properties; the CP-even fields h_1, h_2, σ and the CP-odd fields η_1, η_2, ρ. Since the rotation in eq. (2.20) really transforms the Higgs doublets into each other, it applies also identically to η_1, η_2 and to ϕ_1^+, ϕ_2^+. Therefore, the rotation that

tranforms the real scalar fields $\boldsymbol{\varphi}$ (gauge basis) to the Higgs basis ($\boldsymbol{\varphi}_H$) is given by:

$$\boldsymbol{\varphi}_H = R_0\boldsymbol{\varphi} = \begin{pmatrix} R_1 & 0 \\ 0 & R_1 \end{pmatrix}\boldsymbol{\varphi}^0 \quad \text{where:} \quad R_1 = \begin{pmatrix} \cos\beta & \sin\beta & 0 \\ -\sin\beta & \cos\beta & 0 \\ 0 & 0 & 1 \end{pmatrix} = \begin{pmatrix} \frac{v_1}{v} & \frac{v_2}{v} & 0 \\ -\frac{v_2}{v} & \frac{v_1}{v} & 0 \\ 0 & 0 & 1 \end{pmatrix}, \tag{3.47}$$
$$\text{and} \quad \boldsymbol{\phi}_H = R_+\boldsymbol{\phi} \quad \text{where:} \quad R_+ = \begin{pmatrix} \cos\beta & \sin\beta \\ -\sin\beta & \cos\beta \end{pmatrix}$$

where the form of R_1 reflects the fact that only the fields belonging to Φ_a get rotated. We implicitly introduced the Higgs basis eigenstates, defined as:

$$\boldsymbol{\varphi}_H = \left(H^0, R, \sigma, G^0, I, \rho\right)^T \qquad \boldsymbol{\phi}_H = \left(G^+, H^+\right)^T, \tag{3.48}$$

where we followed standard naming conventions for the Higgs doublet components. Note the components of the scalar singlet are unaffected by this transformation.

Upon spontaneous symmetry breaking, the scalar particles acquire masses from the potential. In the gauge (Lagrangian) basis, the mass matrices are given by [7]:

$$\left[M_0^2\right]_{ij} = \frac{1}{2}\left\langle \frac{\partial^2 V}{\partial\varphi_i\partial\varphi_j} \right\rangle, \qquad \left[M_\pm^2\right]_{ij} = \left\langle \frac{\partial^2 V}{\partial\phi_i\partial\phi_j} \right\rangle. \tag{3.49}$$

The mass terms appear in the Lagrangian as $\mathcal{L}_{\text{mass}} = \frac{1}{2}\varphi_i^T\left[M_0^2\right]_{ij}\varphi_j + \phi_a^\dagger\left[M_\pm^2\right]_{ab}\phi_b$, [8]. The real scalar mass matrix is block-diagonal (as we do not have any CP-violation in the scalar sector). We present the explicit forms of these mass matrices in appendix A. The rotation to the mass basis can be parametrized as a general orthogonal rotation. Since the three parts of the scalar sector do not mix in this model, we will have 3x3 mixing in the CP-even sector, 3×3 in the CP-odd sector and 2×2 in the charged sector.

It is illuminating to consider how transformation to the Higgs basis takes place in practice. Namely:

$$\mathcal{L}_{\text{mass}} = \frac{1}{2}\boldsymbol{\varphi}^{\boldsymbol{T}}M_0^2\boldsymbol{\varphi} = \frac{1}{2}\boldsymbol{\varphi}^{\boldsymbol{T}}R_0^TR_0M_0^2R_0^TR_0\boldsymbol{\varphi} = \frac{1}{2}\boldsymbol{\varphi}^{\boldsymbol{T}}R_0^TM_{0,H}^2R_0\boldsymbol{\varphi} = \frac{1}{2}\boldsymbol{\varphi}_H^{\boldsymbol{T}}M_{0,H}^2\boldsymbol{\varphi}_H \tag{3.50}$$

and similarly for the charged scalars. Here, the new mass matrix of the neutral scalars in the Higgs basis is given by $\left[M_{0,H}\right]^2 = R_0\cdot M_0^2\cdot R_0^T$. Clearly, to change to the mass basis we need to perform a similar transformation with a new block-diagonal transformation matrix O. To rotate to the Higgs basis we needed only one angle, β, that was dictated by the specific requirements that define the Higgs basis. But a general basis transformation will rotate each independent component separately, so we will have an angle for each CP-even and CP-odd component and one angle for the complex charged scalars. Since we have three CP-even and CP-odd components, the corresponding blocks of O need be parametrized as general $\mathsf{SO}(3)$ matrices. The block that diagonalizes the charged sector will be a general $\mathsf{SO}(2)$ matrix since we do not have charged scalar singlet. Explicitly:

$$\boldsymbol{\varphi}_m = O\boldsymbol{\varphi} = \begin{pmatrix} O_1 & 0 \\ 0 & O_2 \end{pmatrix} \qquad \boldsymbol{\phi}_m = O_3\boldsymbol{\phi}, \tag{3.51}$$

where the subscript m denotes the mass basis and:

$$O_1 = O_{x,1}O_{y,1}O_{z,1} = \begin{pmatrix} 1 & 0 & 0 \\ 0 & \cos\theta_1 & \sin\theta_1 \\ 0 & -\sin\theta_1 & \cos\theta_1 \end{pmatrix}\begin{pmatrix} \cos\theta_2 & 0 & -\sin\theta_2 \\ 0 & 1 & 0 \\ \sin\theta_2 & 0 & \cos\theta_2 \end{pmatrix}\begin{pmatrix} \cos\theta_3 & \sin\theta_3 & 0 \\ -\sin\theta_3 & \cos\theta_3 & 0 \\ 0 & 0 & 1 \end{pmatrix}. \tag{3.52}$$

The matrix O_2 has the same form as O_1 but with (potentially) different angles θ_4, θ_5 and θ_6. The last block O_3 is:

$$O_3 = \begin{pmatrix} \cos\theta_7 & \sin\theta_7 \\ -\sin\theta_7 & \cos\theta_7 \end{pmatrix}. \tag{3.53}$$

[7] To understand the origin of the $\frac{1}{2}$ factor, note the number of degrees of freedom in real vs. complex fields (see e.g. [14]).
[8] The mass matrix $M_\pm^2$ and the corresponding mass $m_{H^\pm}$ is the same for both H^+ and $(H^+)^\dagger = H^-$, hence the $\pm$ sign.

We state the names of the mass basis eigenstates:

$$\boldsymbol{\varphi}_m = \left(h, H, \varsigma, G^0, A, \chi\right)^T \qquad \boldsymbol{\phi}_m = \left(G^+, H^+\right)^T . \tag{3.54}$$

We now return to the issue of the Higgs alignment. The condition for Higgs alignment is when the Higgs basis eigenstate, which manifests correct couplings to the vector bosons, is the same as the lightest CP-even mass eigenstate. First observe how the CP-even states are obtained from gauge eigenstates:

$$\begin{pmatrix} H^0 \\ R \\ \sigma \end{pmatrix} = R_1 \begin{pmatrix} h_1 \\ h_2 \\ \sigma \end{pmatrix} \qquad \text{and:} \qquad \begin{pmatrix} h \\ H \\ \varsigma \end{pmatrix} = O_1 \begin{pmatrix} h_1 \\ h_2 \\ \sigma \end{pmatrix}, \tag{3.55}$$

such that:

$$\begin{pmatrix} h \\ H \\ \varsigma \end{pmatrix} = O_1 R_1^T \begin{pmatrix} H^0 \\ R \\ \sigma \end{pmatrix}. \tag{3.56}$$

A schematic illustration of the basis transformations can be found in fig. 2. Introduce $\mathcal{O}_1 = O_1 R_1^T$. The Higgs alignment limit can now we stated as the condition that $[\mathcal{O}_1]_{11} = 1$ (by the orthogonality of $\mathcal{O}_1$ this automatically means that $[\mathcal{O}_1]_{12} = [\mathcal{O}_1]_{13} = [\mathcal{O}_1]_{21} = [\mathcal{O}_1]_{31} = 0$) i.e. $H^0 = h$.

As we shall see in the next section, for the purposes of testing the model on a computer, we are actually interested in the matrices $\mathcal{O}$ rather than O. To figure out how it is to be parametrized we consider what happens in the Higgs basis, since the $\mathcal{O}$ are designed to diagonalize it. In the Higgs basis the Goldstone modes decouple i.e. the corresponding rows and columns in the mass matrix are zero. Therefore, the CP-odd scalar mass matrix is block-diagonal in the Higgs basis with a 2×2 block. Similarly, the G^+ mode is made manifest in the Higgs basis and so the charged scalar mass matrix becomes block diagonal. However, since we only have one other charged scalar state in the model, the charged scalar mass matrix is actually diagonalized in the Higgs basis. Finally, the CP-even scalar mass matrix remains 3×3 with no zero entries. From this we can conclude that the $\mathcal{O}$ matrices can be parametrized as follows: $\mathcal{O}_1$, diagonalizing the CP-even scalars is 3×3 and can be parametrized like eq. (3.52) with angles $\alpha_1, \alpha_2, \alpha_3$; $\mathcal{O}_2$ diagonalizing the CP-odd scalars has a 2×2 block which can be parametrized like eq. (3.53) with angle γ. Explicitly:

$$\boldsymbol{\varphi}_m = \mathcal{O}_0 \boldsymbol{\varphi}_H = \begin{pmatrix} \mathcal{O}_1 & 0 \\ 0 & \mathcal{O}_2 \end{pmatrix} \boldsymbol{\varphi}_H \qquad \text{where:} \qquad \mathcal{O}_2 = \begin{pmatrix} 1 & 0 & 0 \\ 0 & \cos\gamma & \sin\gamma \\ 0 & -\sin\gamma & \cos\gamma \end{pmatrix} \qquad \text{and} \qquad \boldsymbol{\phi}_m = \boldsymbol{\phi}_H . \tag{3.57}$$

Working with the explicit versions of the rotation matrices $\mathcal{O}_1$, allows us to convert the alignment condition $[\mathcal{O}_1]_{11} = 1$ to:

$$\cos\alpha_2 \cos\alpha_3 = 1 \tag{3.58}$$

which, for the purposes our calculations, is satisfied by:

$$\begin{cases} \alpha_1 \in [0, 2\pi) \\ \alpha_2 = 0 \\ \alpha_3 = 0 \end{cases} . \tag{3.59}$$

3.4 Choice of the physical parameters and inversion

Comparing the predictions of a model to experimental data and imposing known restrictions from measurements is best done when the model is expressed in terms of experimentally measurable quantities such as masses and mixing angles. However, in the past sections we have worked predominantly with parameters that appear directly in the Lagrangian - the λ:s and μ:s. We would thus like to rewrite our relations in terms of masses and mixing angles to facilitate straightforward testing of the model numerically.

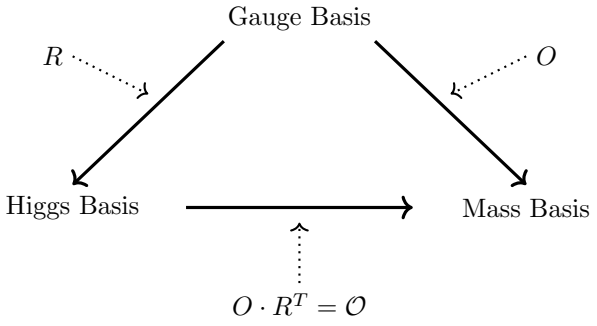

Figure 2: The bases employed in the discussion of the scalar states and the transformation matrices between them.

The last section contains equations relating the gauge basis states to masses and the mass basis. We can use these relations to express as many Lagrangian parameters as possible in terms of masses and angles. From the last sections we can identify and name the following masses:

$$m_h, m_H, m_\varsigma, m_A, m_\chi, m_{H^\pm}. \tag{3.60}$$

The first mass is the SM Higgs boson mass (via the Higgs alignment limit implicitly enforced here) the next mass m_H is a new CP-even Higgs boson. The mass m_ς is the mass state corresponding (predominantly, via mixing) to the CP-even component of the complex singlet. The mass state m_A corresponds to the CP-odd part of the second Higgs doublet that does not become a Goldstone boson. We have the pseudo-Goldstone boson m_χ that acquires its mass through soft-breaking terms. Finally we have the charged Higgs bosons with the same mass $m_{H^\pm}$.

The equality between the mass matrices in the mass basis and the rotated gauge basis mass matrices will give us the necessary equations to solve for the various parameters. For the CP-even states, this equality can be written as:

$$M^2_{diag,1} = O_1 R_1^T R_1 M_0^2 R_1^T R_1 O_1^T = \mathcal{O}_1 R_1 M_0^2 R_1^T \mathcal{O}_1^T = \mathcal{O}_1 M^2_{0,H} \mathcal{O}_1^T, \tag{3.61}$$

where $M^2_{diag,1}$ is the mass matrix of the CP-even scalars in the mass basis. Using the fact that these matrices are block diagonal we get:

$$\begin{aligned} \mathcal{O}_1^T M^2_{diag,1} \mathcal{O}_1 &= R_1 M_0^2 R_1^T \\ \mathcal{O}_2^T M^2_{diag,2} \mathcal{O}_2 &= R_1 M_0^2 R_1^T \\ M^2_{diag,3} &= R_+ M^2_\pm R_+^T, \end{aligned} \tag{3.62}$$

where the added subscripts have the same function as in the last section, namely they discriminate between the sectors (1 - CP-even, 2 - CP-odd and 3 - charged). The rotation matrices $\mathcal{O}_{1,2,3}$ were parametrized explicitly in the last section. If needed, this parametrization can be related to the two sets of rotation matrices R, O.

The reason for the usage of $\mathcal{O}$ and the corresponding transformation between the Higgs and mass bases can now be explained. In the transformation between the Higgs and mass basis we go from a basis where the Goldstone modes are explicit (thus significantly reducing the number of non-zero elements in the matrices) to the diagonal mass basis. Hence we benefit from the partial diagonalization of the Higgs basis.

Since the Goldstone modes appear both in the Higgs and the mass bases, they appear on both sides of the above equations, reducing the size of the matrices. The first equation is thus a 3×3 matrix equation, the second is 2×2 while the third is, as previously mentioned, already diagonalized in the Higgs basis. The mass matrices are symmetric so we have $6 + 3 + 1 = 10$ independent equations. Taking into account which

Lagrangian parameters appear in which sub-matrices, we solve the first 6 equations for λ_1, λ_2, λ_3, λ_1', λ_2' and λ_3'. The next 3 equations are solved for μ_3^2, μ_b^2 and a_1. Finally, we solve the last equation for λ_4. The explicit solutions are presented in appendix B.

So far, we have assumed a strictly obeyed Higgs alignment limit. However, we could relax this requirement by introducing a small misalignment. This way, the physics becomes more interesting while the smallness of the misalignment means that this scenario might reproduce the observed experimental data. To parametrize this scenario consider the upper row of eq. (3.57): $(\cos\alpha_2\cos\alpha_3, \cos\alpha_2\sin\alpha_3, -\sin\alpha_2)$. In the Higgs alignment limit, given by eq. (3.58), the angles $\alpha_{2,3}$ are zero so that only the first element is non-zero. We can instead set the two other, non-diagonal, elements to be equal to some small numbers that will serve to parametrize the off-alignment:

$$\begin{cases} -\sin\alpha_2 & = \delta_2 \quad \Rightarrow \quad \alpha_2 = \arcsin\left(-\delta_2\right), \\ \cos\alpha_2\sin\alpha_3 & = \delta_3 \quad \Rightarrow \quad \alpha_3 = \arcsin\left(\frac{\delta_3}{\cos\alpha_2}\right). \end{cases} \tag{3.63}$$

We conclude this section by summarizing which parameters are considered to be independent in our investigation. The scalar masses in eq. (3.60), the vev mixing angle β, the scalar singlet vev v_s, the CP-odd sector mixing angle γ, the CP-even sector mixing angle α_1 and the two off-alignment parameters δ_2 and δ_3 can be varied independently (within suitably chosen bounds). These constitute the input parameter space in the subsequent numerical analysis.

4 The Yukawa Sector

In this section we explore the Yukawa sector of our model, which is BGL-like. We discuss the parametrization of the textures in section 4.1 and then consider the CKM matrix in section 4.2.

4.1 Inversion procedure

In the scalar sector we were able to conveniently include the experimentally measurable Higgs mass, as well as constraints on SM-like Higgs mixing angle and BSM scalar masses into our model through the so-called inversion procedure. We would like to do the same for the Yukawa sector, trading the Yukawa textures for observable quantities. The latter here are the fermion masses and the CKM matrix (if one would like to test the full νBGL-I model, the lepton mixing matrix (the PMNS matrix) would also have to be included). We will do this through a variant of the procedure outlined in eq. (3.62).

To this end we need, just as in the scalar case, explicit parametrizations of the quark mixing matrices. First, consider the Yukawa textures: the matrix elements can be any complex numbers. To parametrize the Yukawa textures, the idea is to use a relation for e.g. quark masses such as:

$$\mathrm{diag}\left(m_u, m_c, m_t\right) = \left[U_L^u\right]^\dagger M_u U_R^u \tag{4.64}$$

to invert it so that the Yukawa couplings are expressed in terms of the mixings and masses:

$$M_u = U_L^u \cdot \mathrm{diag}\left(m_u, m_c, m_t\right) \cdot \left[U_R^u\right]^\dagger. \tag{4.65}$$

(see section 2.3 for the definition of the notation)[9]. Note that as long as the Yukawa textures are block-diagonal and we have no further conditions on them, the mixing matrices are allowed to be arbitrary *unitary* matrices that respect the block-diagonal structure (i.e. they do only mix the blocks, not between them). In the above example, this means that both U_L^u and U_R^u contain a 2x2 block that is an arbitrary $\mathsf{U}(2)$ matrix and a diagonal complex entry of modulus one.

[9]The astute reader might notice a mismatch in the notation between which mixing matrix is defined as hermitian conjugated here compared to the scalar sector in e.g. eq. (3.50). However this is just a matter of arbitrary naming and does not affect any physics. We follow the convention for the fermion sector of [11] and for the scalar sector of [7].

There are however, additional conditions on the mixing matrices. What is different compared to the scalar case, apart from the complex couplings, is the requirement of the reproduction of the CKM matrix. This means that our fermion mass diagonalization matrices must be such so as to gives us a CKM candidate matrix that is within experimentally determined bounds. For the quarks and their CKM matrix this is straightforward to implement as it turns out, as we can trade the left down-type quark mixing matrix for the CKM matrix as follows:

$$V_{CKM} \equiv [U_L^u]^\dagger U_L^d \qquad \Rightarrow \qquad U_L^d = U_L^u V_{CKM}. \tag{4.66}$$

Using this we can sample the left up-type quark mixing matrix randomly (not worrying about any constraints except those dictated by the family-symmetry) and use the CKM matrix (sampled within experimental bounds) to *calculate* the U_L^d matrix rather than sample it. This way we guarantee the correct quark mixing. Note the following: this is possible since the U_L^d matrix is 3x3 with no additional constraints, in contrast to e.g. U_L^u, we have no conditions that enforce zero-elements in the texture.

Furthermore, we notice that the right mixing matrices are completely arbitrary (except that they must of course be unitary) since they are not observable in any known way (in contrast to the left mixing matrices which enter into the observable CKM matrix).

We can now state the parametrizations that we use for the mixing matrices, which we base on [24]. The most general 2x2 $\mathsf{U}(2)$ matrix has 2^2 degrees of freedom and can be parametrized as:

$$\mathsf{U}(2) \ni A = \begin{pmatrix} 1 & 0 \\ 0 & e^{i(\alpha_{22}-\alpha_{12})} \end{pmatrix} \begin{pmatrix} \cos\theta & \sin\theta \\ -\sin\theta & \cos\theta \end{pmatrix} \begin{pmatrix} e^{i\alpha_{11}} & 0 \\ 0 & e^{i\alpha_{12}} \end{pmatrix}, \tag{4.67}$$

where the four degrees of freedom consist of the three phases $\alpha_{11}, \alpha_{22}, \alpha_{12}$ and the angle θ. Using this, the matrices $U_L^u, U_L^e, U_R^u, U_R^e$ can be parametrized as:

$$U_{L/R}^{u/e} = \begin{pmatrix} A & \mathbf{0} \\ \mathbf{0}^T & e^{i\alpha_{33}} \end{pmatrix}, \tag{4.68}$$

where $\mathbf{0}^T = (0,0)$. The 3x3 matrix U_R^d can be parametrized as:

$$\begin{aligned} \mathsf{U}(3) \ni U_R^d = &\begin{pmatrix} 1 & 0 & 0 \\ 0 & e^{i(\alpha_{23}-\alpha_{13})} & 0 \\ 0 & 0 & e^{i(\alpha_{33}-\alpha_{13})} \end{pmatrix} \begin{pmatrix} c_{12}c_{13} & s_{12}c_{13} & s_{13}e^{-i\delta} \\ -s_{12}c_{23} - c_{12}s_{23}s_{13}e^{i\delta} & c_{12}c_{23} - s_{12}s_{23}s_{13}e^{i\delta} & s_{23}c_{13} \\ s_{12}s_{23} - c_{12}c_{23}s_{13}e^{i\delta} & -c_{12}s_{23} - s_{12}c_{23}s_{13}e^{i\delta} & c_{23}c_{13} \end{pmatrix} \cdot \\ &\cdot \begin{pmatrix} e^{i\alpha_{11}} & 0 & 0 \\ 0 & e^{i\alpha_{12}} & 0 \\ 0 & 0 & e^{i\alpha_{13}} \end{pmatrix}, \end{aligned} \tag{4.69}$$

the 3^2 d.o.f:s are the six phases $\alpha_{11}, \alpha_{12}, \alpha_{13}, \alpha_{23}, \alpha_{33}, \delta$ and the three angles $\theta_{12}, \theta_{13}, \theta_{23}$ that are implicit in the notation $c_{12} = \cos\theta_{12}$. Notice that the middle matrix in eq. (4.69) is the same as the standard parametrization of the CKM matrix [25]. This will be discussed in the next section.

Having specified the explicit parametrizations of the mixing matrices and the equations of the inversion procedure (based on eq. (4.65)) we could now proceed to list the analytical formulas for the Yukawa texture elements. However, while such formulas exist in our scenario (and can be easily obtained using e.g. Mathematica) they are extremely long and have little practical utility. Furthermore, in the computer implementation of this model the matrix inversion of eq. (4.64) to eq. (4.65) is done numerically. We will therefore not list these analytical formulas in the thesis.

4.2 The CKM matrix and the Jarlskog invariant

In the quark sector there are five redundant phases that can be used to remove ("rotate away") five phased in the quark mixing matrices. Usually, it is the phases of the CKM matrix that are removed. As it was observed

earlier, eq. (4.69) has just the form of the CKM matrix except for the *outer* five phases. These are exactly the phases that can be rotated away using the freedom of the quark field phases [24]. One global quark field phase always remains and the last phase of the CKM matrix (δ in the above parametrization) is "hidden" inside the matrix so it can anyway not be rotated away. It is this phase that causes the CP-violation in the quark sector.

A convenient parametrization of the CKM matrix is the Wolfenstein parametrization [26], which we employ in our numerical analysis. In it, the CKM matrix is parametrized as follows:

$$V_{CKM} = \begin{pmatrix} 1-\lambda^2/2 & \lambda & A\lambda^3(\rho - i\eta) \\ -\lambda & 1-\lambda^2/2 & A\lambda^2 \\ A\lambda^3(1-\rho-i\eta) & -A\lambda^2 & 1 \end{pmatrix} + \mathcal{O}\left(\lambda^4\right), \tag{4.70}$$

where the parameters above are defined by:

$$\begin{aligned} s_{12} = \lambda = \frac{|V_{us}|}{\sqrt{|V_{ud}|^2 + |V_{us}|^2}}, \qquad s_{23} = A\lambda^2 = \lambda \left|\frac{V_{cb}}{V_{us}}\right| \\ s_{13}e^{i\delta} = V_{cb}^* = A\lambda^3(\rho + i\eta) = \frac{A\lambda^3\left(\overline{\rho} + i\overline{\eta}\right)\sqrt{1 - A^2\lambda^4}}{\sqrt{1-\lambda^2}\left[1 - A^2\lambda^4\left(\overline{\rho} + i\overline{\eta}\right)\right]}. \end{aligned} \tag{4.71}$$

Here, the LHS of each equality contains quantities from the previously mentioned "standard" parametrization of the CKM, namely the middle matrix of eq. (4.69). The CKM matrix elements are denoted by V_{ij} ($i = u, c, t$ and $j = d, s, b$), where the indices signify the quark flavors to which the matrix element corresponds.

Clearly, the parametrization of the CKM matrix is not unique, neither is the parametrization of the left and right mixing matrices. Among them, there are infinitely many unitary rotations. It is therefore possible to obtain the same physics with different conventions for the matrices. How can we be sure that our method is correct if e.g. one of the programs we employ gives us the same masses but different mixing matrices?

The answer is provided by the Jarlskog invariant [27]. The Jarlskog invariant is given by:

$$J = \mathfrak{Im}\left(V_{us}V_{cb}V_{ub}^*V_{cs}^*\right), \tag{4.72}$$

Two differently parametrized CKM matrices result in the same physics, if the absolute values squared of their matrix elements and their Jarlskog invariants coincide.

5 Implementation

In this section we discuss the more practical aspects of the model investigation. In section 5.1 we present the various constraints that allow us to reject the majority of parameter-points[10] early on in our code, before we employ computationally intensive programs. Then, in section 5.2 we lay out the structure of our software and elaborate on its various components and functions.

5.1 Theoretical and experimental bounds

As will be discussed in section 5.2, our simulations depend on several existing codes that we have linked together. These programs perform a large amount of calculations and are thus very computationally intensive. When performing a numerical investigation like we have done, it is therefore of great interest to exclude as many points as possible using computationally *cheap* constrains before passing the *surviving* points on to the computationally intensive codes. In this subsection we discuss a number of such constraints that we have implemented in our code.

[10] By parameter-point we mean a set of randomly sampled model parameters that exhaust the freedom of the model. Those specific parameters will be specified in section 5.2.

5.1.1 Boundedness from below

The so-called *vacuum stability condition* is the requirement that the scalar potential of any model must be *bounded from below*, i.e. it must not be possible to select a direction in the space spanned by the scalar fields and (eventually) reach states of arbitrarily low energy. This can be conveniently visualized using simple polynomials. A potential given by $V(x) = x^2 - x + C$ is bounded from below, since in both available directions the value of the potential eventually goes up. In contrast, the potential $V(x) = x^3 + x^2$ is not bounded from below, since for sufficiently negative x the value of V decreases without limit. Such a situation is clearly unphysical, therefore any parameter-point exhibiting this property can be promptly rejected. Since the values of the parameter-points that we sample enter the calculation of the coefficients of the terms in the scalar potential, the different values they assume can lead to very different geometries featuring both bounded from below and unbounded potentials.

In this section we follow the method for ensuring boundedness from below presented in [28]. We will not derive all the results leading up to the criteria, the interested reader is referred to the aforementioned paper. The condition of boundedness from below can be ensured by the so called co-positivity criterion on the matrix of quartic couplings. We need only to consider the quartic couplings since their dimension four terms dominate the behavior of the potential for large field-values. Following the convention of [28], our matrix of quartic couplings is:

$$\Lambda = \begin{pmatrix} \lambda_1 & \frac{1}{2}\left(\lambda_3 + \lambda_4\rho^2\right) & \frac{1}{2}\lambda_2' \\ \frac{1}{2}\left(\lambda_3 + \lambda_4\rho^2\right) & \lambda_2 & \frac{1}{2}\lambda_3' \\ \frac{1}{2}\lambda_2' & \frac{1}{2}\lambda_3' & \lambda_1' \end{pmatrix}, \tag{5.73}$$

where the parameter ρ can take on the following values: $\rho \in [0, 1]$. From this matrix the co-positivity criteria can be read off. They are:

$$\begin{aligned} &\lambda_1 \geq 0 \quad \lambda_2 \geq 0 \quad \lambda_1' \geq 0 \\ &\overline{\lambda_1} = \frac{1}{2}\left(\lambda_3 + \Theta\left(-\lambda_4\right)\lambda_4\right)\sqrt{\lambda_1\lambda_2} \geq 0 \quad \overline{\lambda_2} = \frac{1}{2}\lambda_2' + \sqrt{\lambda_1\lambda_1'} \geq 0 \quad \overline{\lambda_3} = \frac{1}{2}\lambda_3' + \sqrt{\lambda_2\lambda_1'} \geq 0 \\ &\sqrt{\lambda_1\lambda_2\lambda_1'} + \frac{1}{2}\left(\lambda_3 + \Theta\left(-\lambda_4\right)\lambda_4\right)\sqrt{\lambda_1'} + \frac{1}{2}\lambda_2'\sqrt{\lambda_2} + \frac{1}{2}\lambda_3'\sqrt{\lambda_1} + \sqrt{2\overline{\lambda_1}\cdot\overline{\lambda_2}\cdot\overline{\lambda_3}} \geq 0, \end{aligned} \tag{5.74}$$

where $\Theta(x) = \begin{cases} 1, \text{ if } x > 0 \\ 0, \text{ if } x < 0 \end{cases}$ is the Heaviside step function. In our simulations, all points that do not satisfy all of these conditions are rejected.

5.1.2 Tree-Level unitarity of the scattering matrix

One of the most important checks that a candidate point must pass is the unitarity of the scalar elastic two-body scattering matrix (S-matrix) [29, 18]. This means that in the high energy limit, the tree-level S-matrix of all possible two-body elastic scalar boson scatterings must remain unitary (for the parameter values specified).

Following [30], this requirement can be translated into a condition on the Jth partial wave a^J by utilizing the optical theorem:

$$\mathfrak{Im}\left(a^J\right) = \left|a^J\right|^2 \quad \Rightarrow \quad \left|\mathfrak{Re}\left(a^J\right)\right| \leq \frac{1}{2}, \tag{5.75}$$

where the implication follows upon recognition that the first equation is an equation for a circle in the complex plane. In the high energy limit only the four-point interactions contribute to these two-to-two scatterings.

The partial wave amplitude for $J = 0$ is related to the transition matrix element of the four-point scatterings by [31]:

$$a_{ij}^0 = \frac{1}{16\pi}\left\langle\Omega_i|i\hat{T}^0|\Omega_j\right\rangle, \tag{5.76}$$

where Ω_i, Ω_j are the in-going and out-going two-particle states and $\hat{T}^0$ is the $J = 0$ contribution to the transition matrix of the process. Upon setting up a suitable basis for the in- and out-going states, that exhausts all the possibilities in the model, the above formula can be used to straightforwardly compute the full scattering matrix (subject to, of course, the conditions of tree-level only, 2 to 2 elastic scatterings). The unitarity condition eq. (5.75) takes the form:

$$\langle \Omega_i | i\hat{T}^0 | \Omega_j \rangle \leq 8\pi. \tag{5.77}$$

The task of computing the unitarity limits now reduces to finding the eigenvalues of the $\langle \Omega_i | i\hat{T}^0 | \Omega_j \rangle$ matrix. Since we could not find any previous research where such unitarity bounds had been calculated for a scalar sector such as the one investigated in this work, the derivation of the unitarity bounds has to be performed independently. The authors of [32] outline in their paper an algorithm for the calculation of those eigenvalues for a wide class of scalar models. As a part of this project, we adapt this algorithm to our model and implement it in MATHEMATICA. The crucial step in calculating such bounds is to set up a suitable basis of states Ω_i, Ω_j. In table 2 we present our adaptation of the basis of states utilized in [32]. The authors of said paper classify the states according to quantum numbers that are conserved in the scatterings under consideration: electric charge Q and weak hypercharge Y. To this end, the states are constructed using complex fields rather than the separated real constituents.

Table 2: *The states used in the calculation of the unitarity limits on the scattering matrix. Note that apart from these, their hermitian conjugates are also to be included in the calculation. We have here adopted the naming convention of the original paper [32] wherever applicable. The translation to our naming convention reads:* $w_i^+ = \phi_i^+$ *and* $n_i = \frac{1}{\sqrt{2}}(h_i + i\eta_i)$

Q	2Y	States
2	2	$S_\alpha^{++} = w_i^+ w_J^+$
1	2	$S_\alpha^{+} = w_i^+ n_j$
1	1	$N_\alpha^{++} = \{w_i^+ \sigma, w_i^+ \mathcal{S}^*\}$
1	0	$T_\alpha^{+} = w_i^+ n_j^*$
0	2	$S_\alpha^{0} = n_i n_j^*$
0	1	$N_\alpha^{+} = \{n_i \mathcal{S}, n_i \mathcal{S}^*\}$
0	0	$T_\alpha^{0} = \{w_i^- w_j^+, n_i n_j^*, \mathcal{S}\mathcal{S}^*\}$

The algorithm is described in detail in the source paper [32] and will not be presented here. Our MATHEMATICA implementation yields the following eigenvalues of the two-to-two elastic scalar scattering matrix:

$$y_i \in \{2\lambda_1, 2\lambda_2, 2\lambda_1', \lambda_3, \lambda_4, \lambda_2', \lambda_3', \lambda_3 + 2\lambda_4, \lambda_3 + \lambda_4, \lambda_3 - \lambda_4, \lambda_1 + \lambda_2 \pm \sqrt{\lambda_1^2 - 2\lambda_1\lambda_2 + \lambda_2^2 + \lambda_4^2}\} \tag{5.78}$$

and in addition, the three roots of:

$$\begin{aligned} 0 = {} & x^3 - x^2\left(4\lambda_1 + 4\lambda_2 + 2\lambda_1'\right) + x\left(8\lambda_1\lambda_1' + 16\lambda_1\lambda_2 + 8\lambda_1'\lambda_2 - 2\lambda_2'^2 - 4\lambda_3^2 - 2\lambda_3'^2 - 4\lambda_3\lambda_4 - \lambda_4^2\right) + \\ & + 2\lambda_1'\lambda_4^2 - 4\lambda_2'\lambda_3'\lambda_4 + 8\lambda_1'\lambda_3\lambda_4 - 8\lambda_1\lambda_3'^2 - 8\lambda_2'\lambda_3'\lambda_4 + 8\lambda_1'\lambda_3^2 + 8\lambda_2\lambda_2'^2 - 32\lambda_1\lambda_1'\lambda_2. \end{aligned} \tag{5.79}$$

The unitarity of the S-matrix (at tree level) is ensured by requiring that none of these eigenvalues exceeds 8π in absolute value (the application of eq. (5.77)).

5.1.3 Electroweak precision observables

The effects of NP on electroweak precision observables can, under suitable conditions be parametrized using the oblique correction parameters S, T, U [33]. Since our model fulfills these criteria and the bounds on the oblique parameters are readily available [25] they offer a perfect opportunity to veto candidate points. Following [33], we adapt and implement the formulas for the S, T, U parameters contained therein.

As with the previous two types of bounds discussed above, we do not present the full formulas that give us the bounds. Instead we show below the formula for one of the oblique parameters (T) and discuss the implementation, the interested reader can consult the original paper [33] to find the full expressions. The parameter T is given by:

$$\begin{aligned}\alpha T \equiv \overline{T} = \frac{g^2}{64\pi^2 m_W^2}\Bigg\{&\sum_{a=2}^{n}\sum_{b=2}^{m}\left|\left(\mathcal{U}^\dagger\mathcal{V}\right)_{ab}\right|^2 F\left(m_a^2,\mu_b^2\right) - \sum_{b=2}^{m-1}\sum_{b'=b+1}^{m}\left[\mathfrak{Im}\left(\mathcal{V}^\dagger\mathcal{V}\right)_{bb'}\right]^2 F\left(\mu_b^2,\mu_{b'}^2\right) + \\ &- 2\sum_{a=2}^{n-1}\sum_{a'=a+1}^{n}\left|\left(\mathcal{U}^\dagger\mathcal{U}\right)_{aa'}\right|^2 F\left(m_a^2,m_{a'}^2\right) + 3\sum_{b=2}^{m}\left[\mathfrak{Im}\left(\mathcal{V}^\dagger\mathcal{V}\right)_{1b}\right]^2\left[F\left(m_Z^2,\mu_b^2\right) - F\left(m_W^2,\mu_b^2\right)\right] + \\ &- 3\left[F\left(m_Z^2,m_h^2\right) - F\left(m_W^2,m_h^2\right)\right]\Bigg\},\end{aligned} \tag{5.80}$$

where α is the fine structure constant, g is the weak force coupling, m_Z, m_W, m_h refer to the $W^\pm$, Z^0 and SM Higgs bosons respectively, m_a denote the neutral scalar masses and lastly, μ_b denote charged scalar masses (in our case only one such mass: $m_{H^\pm}$). The function F is given below:

$$F(I,J) \equiv \begin{cases} \frac{I+J}{2} - \frac{IJ}{I-J}\ln\frac{I}{J} & \text{if } I \neq J \\ 0 & \text{if } I = J. \end{cases} \tag{5.81}$$

Next, we translate the $\mathcal{U}$ and $\mathcal{V}$ matrices to our convention. In the source article, they are defined as the (complex) matrices that take the mass eigenstates (charged and neutral, respectively) to gauge eigenstates. We note that the matrix $\mathcal{U}$ is the same as the transpose of our R_+. The matrix $\mathcal{V}$ acts on complex neutral states, while we work with real neutral fields. To express the $\mathcal{V}$ matrix in terms of our matrices we note that (introducing the matrix $\mathcal{R}$ which fulfills the same function as $\mathcal{V}$ but for the gauge singlet states):

$$\begin{pmatrix}\mathfrak{Re}\mathcal{V}\\ \mathfrak{Im}\mathcal{V}\\ \mathcal{R}\end{pmatrix}\begin{pmatrix}h\\H\\G^0\\A\\\varsigma\\\chi\end{pmatrix} = \begin{pmatrix}h_1\\h_2\\\eta_1\\\eta_2\\\sigma\\\rho\end{pmatrix} \quad\Rightarrow\quad \begin{pmatrix}h\\H\\G^0\\A\\\varsigma\\\chi\end{pmatrix} = \begin{pmatrix}\mathfrak{Re}\mathcal{V}\\ \mathfrak{Im}\mathcal{V}\\ \mathcal{R}\end{pmatrix}^T\begin{pmatrix}h_1\\h_2\\\eta_1\\\eta_2\\\sigma\\\rho\end{pmatrix} \tag{5.82}$$

and using this we find $\mathcal{V}$ by relating the above basis-changing matrix to our matrices O_1, O_2 (see fig. 2). We find:

$$\begin{pmatrix}\mathfrak{Re}\mathcal{V}\\ \mathfrak{Im}\mathcal{V}\\ \mathcal{R}\end{pmatrix}^T = \begin{pmatrix} [O_1]_{11} & [O_1]_{12} & 0 & 0 & [O_1]_{13} & 0 \\ [O_1]_{21} & [O_1]_{22} & 0 & 0 & [O_1]_{23} & 0 \\ 0 & 0 & [O_2]_{11} & [O_2]_{12} & 0 & [O_2]_{13} \\ 0 & 0 & [O_2]_{21} & [O_2]_{22} & 0 & [O_2]_{23} \\ [O_1]_{31} & [O_1]_{32} & 0 & 0 & [O_1]_{33} & 0 \\ 0 & 0 & [O_2]_{31} & [O_2]_{32} & 0 & [O_2]_{33} \end{pmatrix}, \tag{5.83}$$

which is simply a rearrangement of the matrices that take the gauge basis to the mass basis, such that the gauge eigenstates that do not couple to the weak vector bosons (and thus do not contribute to S, T, U) are separated.

5.1.4 Higgs physics constraints

Since the model we are considering features multiple scalar particles and since there both are and have been experiments looking for such extra scalars, it is important to compare the model predictions to experimental data. Apart from the 125 GeV Higgs particle h detected at LHC [1, 2], there have been no confirmed sightings of any extra scalars. Therefore, whatever the predictions of our model may be, all parameter points that do not agree with the published experimental exclusion bounds have to be promptly rejected.

To manually collect and correctly compare all the available experimental data would be a prohibitively time-consuming task. However, the publicly available code HiggsBounds (HB) [34, 35, 36, 37, 38] automatically performs this function, namely it compares the model predictions to 95% confidence limit (C.L.) exclusion bounds from LEP, Tevatron and LHC searches.

A brief description of the workings of HB follows. An important concept in the realm of Higgs physics constraints is the *signal topology* X. Is is defined as a combination of a particular production process of one or two scalar particles $P(h)$ or $P(h_1, h_2)$ and specific decay mode(s) F. The results published by the experimental collaborations can be divided into two types: model-independent bounds on specific signal topologies and combined analyses designed to constrain certain popular models (e.g. the SM and the Minimal Supersymmetric Standard Model (MSSM)). The latter type of bounds are usually stricter but cannot be straightforwardly applied to other models due to the in-built model assumptions. The HB tests whether the supplied parameter point is sufficiently similar to one of the models for which the combined analyses have been performed, and depending on the answer compares it to the different available bounds.

The basic principle of the comparison of the parameter point data to the experimental exclusion bounds is the following. The data needed by the program is the masses of the scalar bosons (including specification of which of them are neutral and which charged), their total decay widths, their decay branching ratios and production cross sections (normalized to a reference value). The programs first determines which signal topology has the highest statistical sensitivity, X_0, by calculating:

$$X_0 = X : \max \left\{ \frac{Q_{\text{model}}(X)}{Q_{\text{expec}}(X)} \right\}, \tag{5.84}$$

where $Q(X)$ denotes the cross section for the signal topology X. "Model" refers to the prediction of the the parameter point (the model under consideration) and is calculated from the required input data. "Expec" stands for the expected 95% C.L. exclusion limit on $Q(X)$ as obtained from Monte Carlo simulations. The model prediction for the most sensitive topology is then compared to experimental data by evaluating the ratio:

$$\frac{Q_{\text{model}}(X_0)}{Q_{\text{obs}}(X_0)}, \tag{5.85}$$

where "obs" refers to the experimentally established 95% exclusion limit on the signal cross section. If this ratio is greater than one, the point is excluded at 95% C.L. The program features many input options that are described in the above cited references. In particular, there is an option to provide effective couplings rather than production cross sections as input. This option is used by us, since such couplings can be automatically calculated by another program that we employ, SPheno [39, 40].

Following the celebrated discovery of a Higgs particle candidate in 2012, a sister program to HB was developed, HiggsSignals (HS) [41]. Its task is to compare the predictions of the model, in the form of signal strength modifiers, to the signal strength modifiers obtained experimentally. The signal strength modifier is a quantitative measure of the model (or observed) signal strength, normalized to the SM prediction. To carry out the comparison, two complementary χ^2 measures are computed by the HS to obtain a quantitative answer to the question how compatible the parameter point is with the experimental Higgs signal.

5.2 Numerical analysis

The goal of the numerical analysis is to perform a random scan over the free parameters of the model (from the scalar and Yukawa sectors) and investigate which of the sampled points pass various relevant bounds. The implementation of the bounds is made in such a way, that the computationally cheapest bounds (discussed in section 5.1) are implemented so that they reject failing points before the rest of the codes are employed. Upon passing the aforementioned first checks, a candidate point passes onto SPheno which calculates the mass spectrum, mixing matrices, Wilson coefficients, branching ratios and more. To configure SPheno for our model, we use a Mathematica package, SARAH [42], where we implement our model and use it to set-up SPheno. The output data of SPheno is used to start HiggsBounds which in turn provides the necessary input for HiggsSignals. The final output of this chain of codes is thus parameter points that

have passed both the HiggsBounds and HiggsSignals checks, in addition to the boundedness from below, unitarity and S, T, U bounds.

The constraints from flavor physics are implemented a posteriori during the analysis stage. The saved Wilson coefficients computed by SPheno in conjunction with FlavorKit [43] are used to calculate flavor physics observables using the python package flavio [44]. The results of these analyses are presented in section 6.

For a more technical description of the codes, see appendix C.

The early results we obtained motivated us to consider the Jarlskog invariant, presented in section 4.2. We noticed that the mixing matrices given by SPheno gave a different CKM matrix than the one constructed from the mixing matrices as sampled by our program. Upon investigation however, we found that the two matrices agree according to the criteria discussed in section 4.2.

5.2.1 Input parameter space

The numerical input values that enter our simulations are documented in this section. For all fermion and gauge boson masses as well as CKM matrix entries and uncertainties (Wolfenstein parametrization), oblique parameter values and the experimentally detected Higgs boson mass we use the values provided by the Particle Data Group [25] (2021 update). All the angles and phases in the Yukawa inversion are allowed to vary within $[0, 2\pi)$. For the other input parameters, we use the values displayed in table 3.

Table 3: *The intervals in which the various parameters are sampled. X in the first entry refers to all of the following: $H, A, \varsigma, \chi, H^+$.*

m_X [GeV]	v_s [GeV]	α_1	γ	δ_2 & δ_3	β
[80, 500]	[100, 500]	$[0, 2\pi)$	$[0, 2\pi)$	(-0.2, 0.2)	$[0, \frac{\pi}{2})$

6 Results

We begin with the presentation of plots depicting the oblique parameter values of the sampled parameter points. In fig. 3 we plot S vs T while in fig. 4 we plot U vs T. In both cases we plot both a representable sample of failed points (points having been rejected either due to HB, HS or any one of the pre-SPheno bounds discussed in section 5.1) and the points that have passed all checks including HB & HS (but excluding any flavor physics limits). Note that the proportion of the failed to successful points is not representative of the scanning procedure. In the aforementioned plots we have about 1000 successful points and 10000 failed ones. However, in the scanning procedure there were of the order of 10 million failed points per the 1000 successful ones. The experimental bounds on the oblique parameters, as provided by [25], are also shown in said plots. They clearly show how efficiently the implementation of these bounds restrict the parameter space: the vast majority of depicted points fall outside these bounds and were thus rejected at an early stage of the scanning procedure. In addition, we see that the T parameter varies considerably more than S and U. This is expected, as described in [33].

We now shift our attention to the flavor physics considerations. The reason behind considering the BGL-model is to provide a mechanism for suppression of FCNC:s. We have calculated a representative sample of related observables using the flavio package, in what follows we present the most interesting ones. To determine whether a point is to be rejected or not based on flavor physics analysis, we have computed 1 σ C.L. using experimental data from [25] and the the flavio package. These limits are shown in all the following plots. We reject a point if it falls outside said bounds. We find that the model obeys several key observables with good margins, while the bounds on other observables result in a rejection of a large portion of the points that otherwise pass all the other bounds and checks.

Among the observables that the model easily satisfies we find the branching ratio fractions $\frac{\mathrm{BR}\left(K_+ \to \pi^+ \nu\overline{\nu}\right)}{\mathrm{BR}_{\ \mathrm{SM}}(K_+ \to \pi^+ \nu\overline{\nu})}$ and $\frac{\mathrm{BR}(B \to X_s\gamma)}{\mathrm{BR}_{\mathrm{SM}}(B \to X_s\gamma)}$ which are shown in fig. 5. The parameter $|\epsilon|$ of the kaon system is also well under control

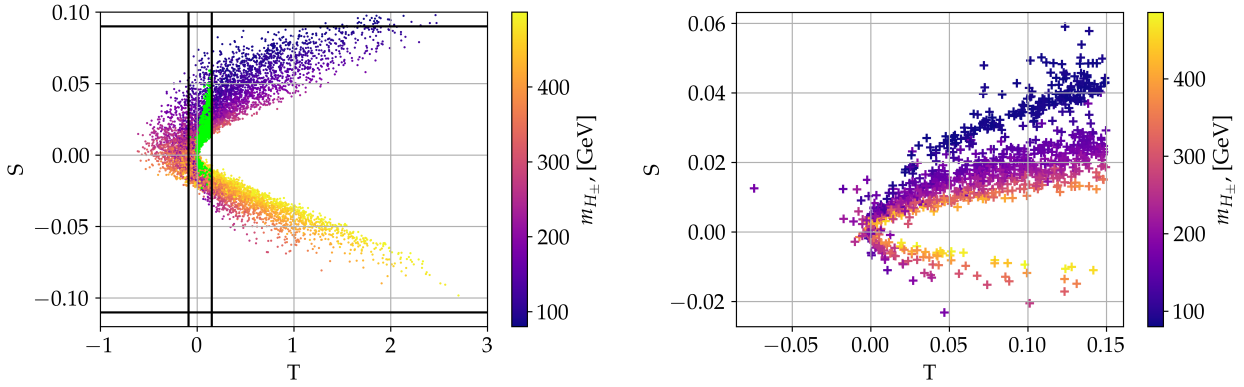

(a) Including failed points.

(b) Only points passing HB & HS.

Figure 3: The oblique parameters S and T. In subplot a) we have plotted their values for a representative sample of points that failed at least one bound. The black vertical and horizontal lines are the experimental bounds from [25]. The green points are those that passed HB & HS. They are shown separately in subplot b).

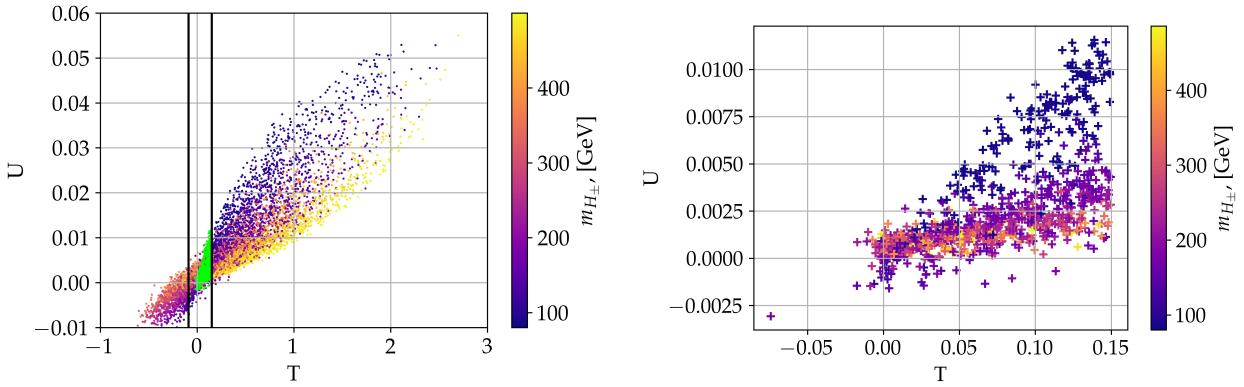

(a) Including failed points.

(b) Only points passing HB & HS.

Figure 4: The oblique parameters U and T. In subplot a) we have plotted their values for a representative sample of points that failed at least one bound. The black vertical and horizontal lines are the experimental bounds from [25]. The green points are those that passed HB & HS. They are shown separately in subplot b).

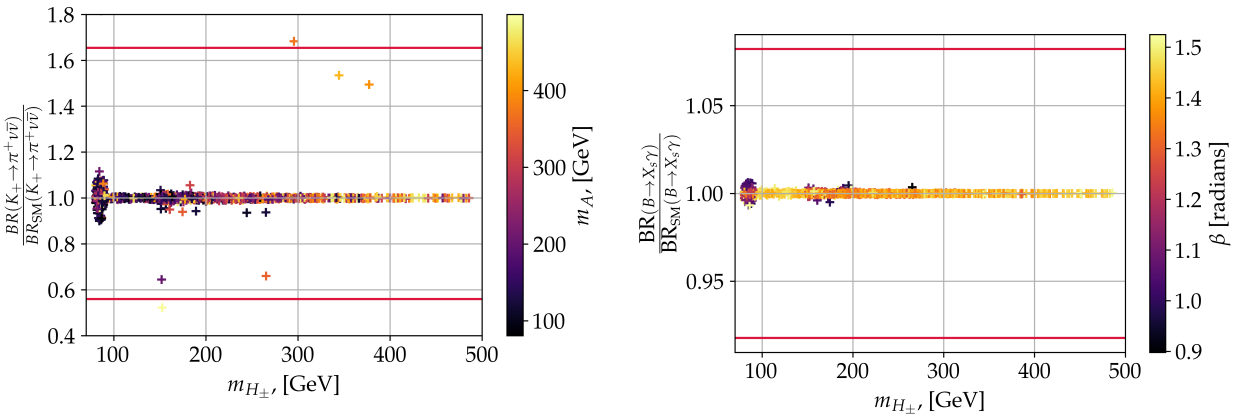

(a) $\frac{\mathrm{BR}\left(K_+\to\pi^+\nu\bar{\nu}\right)}{\mathrm{BR}_{\mathrm{SM}}\left(K_+\to\pi^+\nu\bar{\nu}\right)}$ (b) $\frac{\mathrm{BR}(B\to X_s\gamma)}{\mathrm{BR}_{\mathrm{SM}}(B\to X_s\gamma)}$

Figure 5: Flavor observables that are well within 1σ C.L. In subplot a), $\frac{\mathrm{BR}\left(K_+\to\pi^+\nu\bar{\nu}\right)}{\mathrm{BR}_{\mathrm{SM}}(K_+\to\pi^+\nu\bar{\nu})}$. In fig. 5b, $\frac{\mathrm{BR}(B\to X_s\gamma)}{\mathrm{BR}_{\mathrm{SM}}(B\to X_s\gamma)}$.

in the model, as can be seen in fig. 6. Here, we also plotted this observable against the vev v_2 to show the hierarchical selection of vev allocation that the model displays. All the points passing HB & HS have most of the value of v in the second Higgs doublet [11]. This can be understood on the basis of the Yukawa couplings: the second doublet is (mostly) responsible for giving the mass to the heavy fermions. As can be seen from eq. (2.22), maximizing v_2 leads then to a minimization of the top quark coupling to the extra scalars, which makes them harder to produce at colliders hence allowing more such points to pass HB & HS.

Some other flavor observables result in many rejected points. In fig. 7 the branching ratio fractions $\frac{\mathrm{BR}\left(B_0\to\mu^+\mu^-\right)}{\mathrm{BR}_{SM}(B_0\to\mu^+\mu^-)}$ and $\frac{\mathrm{BR}\left(B_s\to\mu^-\mu^+\right)}{\mathrm{BR}_{\mathrm{SM}}(B_s\to\mu^-\mu^+)}$ are shown. We see that in particular for the second observable, a majority of points is rejected including almost all the low-mass scalars (from fig. 7b we explicitly see this for $H^\pm$ and A). Similarly restricting are the observables $\frac{\Delta M_d}{\Delta M_d(SM)}$ and $\frac{\Delta M_s}{\Delta M_s(SM)}$ shown in fig. 8.

7 Conclusions

In this project, we have studied a scalar singlet and Higgs doublet extended SM with BGL-like suppression of FCNS:s in the quark sector and a simple lepton sector. In order to ensure the exploration of as large an area of uncharted physics territory as possible, we facilitated our analysis with the most general Yukawa textures and mixing matrices in the quark sector as well as with a relaxed Higgs-alignment limit. To optimize the code, we implemented three different checks for rejecting large numbers of parameter points at a stage before the employment of heavier, public, programs. These were boundedness from below, for which we derived necessary and sufficient conditions, unitarity of the scattering matrix, where we obtained tree-level analytical conditions and checks of electroweak precision observables via the STU parameters. This resulted in a significant performance boost.

The parameter space scan resulted in passing points with scalar masses spread out over the entire 80-500 GeV scan range. In particular, there was a concentration of charged Higgses with masses at about 80 GeV. Upon implementing the complementary flavor physics analysis however, most of such points were rejected. The flavor observables that were particularly limiting turned out to be ΔM_d, ΔM_s and $\mathrm{BR}\left(B_s\to\mu^-\mu^+\right)$. In general however, the BGL-like nature of the model was evident, as many other flavor observables that were studied were well within their 1 σ bounds and there was a significant number of points passing all constraints.

[11] This one figure suffices to show this, since all the other plots showcase the same points, just for different observables

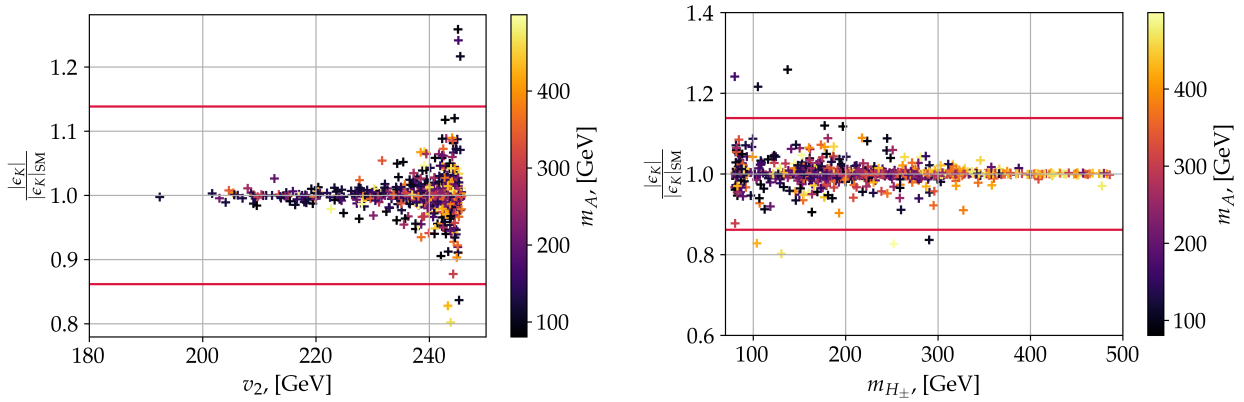

(a) $\frac{|\epsilon|}{|\epsilon|_{\rm SM}}$ (b) $\frac{|\epsilon|}{|\epsilon|_{\rm SM}}$

Figure 6: Flavor observables that are well within 1σ C.L. In subplot a), $\frac{|\epsilon|}{|\epsilon|_{\rm SM}}$ plotted vs v_2. In fig. 5b, $\frac{|\epsilon|}{|\epsilon|_{\rm SM}}$ again, this time plotted against $m_{H_\pm}$.

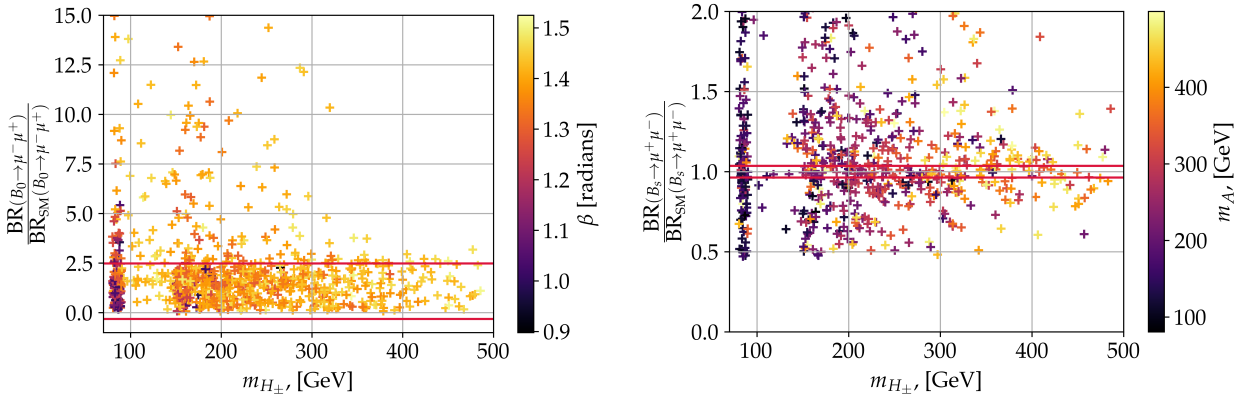

(a) $\frac{\mathrm{BR}\left(B_0\to\mu^+\mu^-\right)}{\mathrm{BR}_{SM}\left(B_0\to\mu^+\mu^-\right)}$ (b) $\frac{\mathrm{BR}\left(B_s\to\mu^-\mu^+\right)}{\mathrm{BR}_{\rm SM}\left(B_s\to\mu^-\mu^+\right)}$

Figure 7: Two flavor observables that result in plenty of rejected points. In fig. 7a, $\frac{\mathrm{BR}\left(B_0\to\mu^+\mu^-\right)}{\mathrm{BR}_{SM}\left(B_0\to\mu^+\mu^-\right)}$. In fig. 7b, $\frac{\mathrm{BR}\left(B_s\to\mu^-\mu^+\right)}{\mathrm{BR}_{\rm SM}\left(B_s\to\mu^-\mu^+\right)}$.

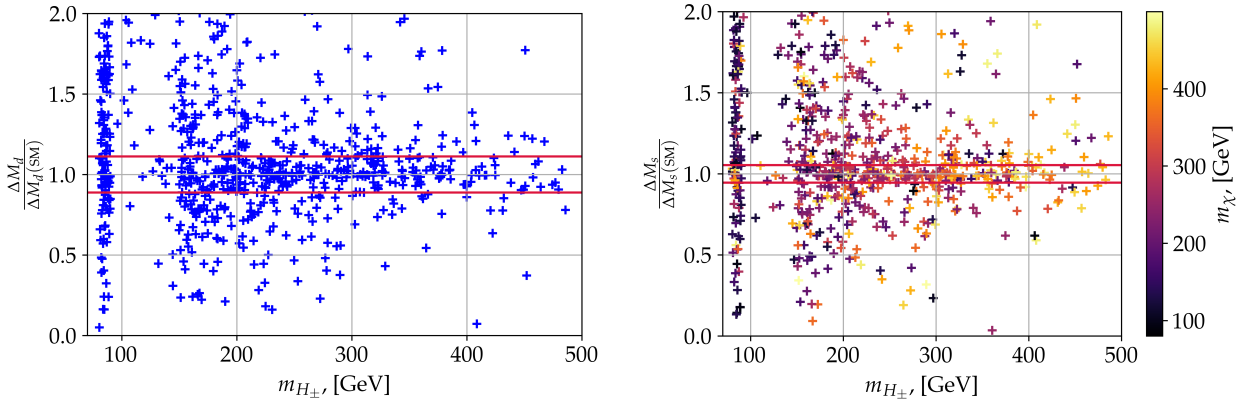

(a) $\frac{\Delta M_d}{\Delta M_d(SM)}$ (b) $\frac{\Delta M_s}{\Delta M_s(SM)}$

Figure 8: Two flavor observables that result in plenty of rejected points. In fig. 8a, $\frac{\Delta M_d}{\Delta M_d(SM)}$. In fig. 8b, $\frac{\Delta M_s}{\Delta M_s(SM)}$.

Acknowledgments

Firstly, I would like to thank my supervisor Roman Pasechnik for his guidance and patience throughout the year. I am grateful to my co-supervisor António Morais for many helpful discussions and remarks. Many thanks to my family and friends for showing support and understanding during this tough year. A special thanks to Felipe Freitas for his lectures on neural networks and finally, a big thank you to Vasileios Vatellis for the close collaboration that we have had and the generous sharing of his experience.

A Mass Matrices

In this appendix we present the symmetric mass matrices of the scalar sector. In the gauge basis, we have for the CP-even scalars:

$$M^2_{0,\mathrm{even}} = \begin{pmatrix} \left[M^2_{0,\mathrm{even}}\right]_{11} & \left[M^2_{0,\mathrm{even}}\right]_{12} & \left[M^2_{0,\mathrm{even}}\right]_{13} \\ \left[M^2_{0,\mathrm{even}}\right]_{12} & \left[M^2_{0,\mathrm{even}}\right]_{22} & \left[M^2_{0,\mathrm{even}}\right]_{23} \\ \left[M^2_{0,\mathrm{even}}\right]_{13} & \left[M^2_{0,\mathrm{even}}\right]_{23} & \left[M^2_{0,\mathrm{even}}\right]_{33} \end{pmatrix}, \tag{A.1}$$

where the elements are:

$$\begin{aligned}
\left[M^2_{0,\mathrm{even}}\right]_{11} &= 3v_1^2\lambda_1 + \frac{1}{2}\left(v_s^2\lambda'_2 + v_2^2\lambda_3 + v_2^2\lambda_4 - \frac{1}{v_1}\left[a_1 v_2 v_s\sqrt{2} + 2v_1^3\lambda_1 + v_1 v_s^2\lambda'_2 + v_1 v_2^2\lambda_3 + v_1 v_2^2\lambda_4 + 2v_2\mu_3^2\right]\right), \\
\left[M^2_{0,\mathrm{even}}\right]_{12} &= \frac{1}{\sqrt{2}}a_1 v_s + v_1 v_2\lambda_3 + v_1 v_2\lambda_4 + \mu_3^2, \\
\left[M^2_{0,\mathrm{even}}\right]_{13} &= \frac{1}{\sqrt{2}}a_1 v_2 + v_1 v_s\lambda'_2, \\
\left[M^2_{0,\mathrm{even}}\right]_{22} &= 3v_2^2\lambda_2 + \frac{1}{2}\left(v_s^2\lambda'_3 + v_1^2\lambda_3 + v_1^2\lambda_4 - \frac{1}{v_2}\left[a_1 v_1 v_s\sqrt{2} + 2v_2^3\lambda_2 + v_2 v_s^2\lambda'_3 + v_1^2 v_2\lambda_3 + v_1^2 v_2\lambda_4 + 2v_1\mu_3^2\right]\right), \\
\left[M^2_{0,\mathrm{even}}\right]_{23} &= \frac{1}{\sqrt{2}}a_1 v_1 + v_2 v_s\lambda'_3, \\
\left[M^2_{0,\mathrm{even}}\right]_{33} &= 3v_s^2\lambda'_1 + \frac{1}{2}\left(v_1^2\lambda'_2 + v_2^2\lambda'_3 + 2\mu_b^2 - \frac{1}{v_s}\left[a_1 v_2 v_2\sqrt{2} + 2v_s^3\lambda'_1 + v_1^2 v_s\lambda'_2 + v_2^2 v_s\lambda'_3 + 2v_s\mu_b^2\right]\right).
\end{aligned} \tag{A.2}$$

For the CP-odd scalars:

$$M^2_{0,\text{odd}} = \begin{pmatrix} \left[M^2_{0,\text{odd}}\right]_{11} & \left[M^2_{0,\text{odd}}\right]_{12} & \left[M^2_{0,\text{odd}}\right]_{13} \\ \left[M^2_{0,\text{odd}}\right]_{12} & \left[M^2_{0,\text{odd}}\right]_{22} & \left[M^2_{0,\text{odd}}\right]_{23} \\ \left[M^2_{0,\text{odd}}\right]_{13} & \left[M^2_{0,\text{odd}}\right]_{23} & \left[M^2_{0,\text{odd}}\right]_{33} \end{pmatrix}, \tag{A.3}$$

where the elements are:

$$\begin{aligned} \left[M^2_{0,\text{odd}}\right]_{11} &= \left[M^2_{0,\text{even}}\right]_{11} - 2v_1^2\lambda_1, \\ \left[M^2_{0,\text{odd}}\right]_{12} &= \frac{1}{\sqrt{2}}a_1 v_s + \mu_3^2, \\ \left[M^2_{0,\text{odd}}\right]_{13} &= \frac{1}{\sqrt{2}}a_1 v_2, \\ \left[M^2_{0,\text{odd}}\right]_{22} &= \left[M^2_{0,\text{even}}\right]_{22} - 2v_2\lambda_2, \\ \left[M^2_{0,\text{odd}}\right]_{23} &= -\frac{1}{\sqrt{2}}a_1 v_1, \\ \left[M^2_{0,\text{odd}}\right]_{33} &= \left[M^2_{0,\text{even}}\right]_{33} - 2v_s^2\lambda_1' - \frac{3}{2}\mu_b^2. \end{aligned} \tag{A.4}$$

For the charged scalars:

$$M^2_{\pm} = \begin{pmatrix} \left[M^2_{\pm}\right]_{11} & \left[M^2_{\pm}\right]_{12} \\ \left[M^2_{\pm}\right]_{12} & \left[M^2_{\pm}\right]_{22} \end{pmatrix}, \tag{A.5}$$

where the elements are:

$$\begin{aligned} \left[M^2_{\pm}\right]_{11} &= v_1^2\lambda_1 + \frac{1}{2}\left(v_s^2\lambda_2' + v_2^2\lambda_3 - \frac{1}{v_1}\left[a_1 v_2 v_s\sqrt{2} + 2v_1^3\lambda_1 + v_1 v_s^2\lambda_2' + v_1 v_2^2\lambda_3 + v_1 v_2^2\lambda_4 + 2v_2\mu_3^2\right]\right), \\ \left[M^2_{\pm}\right]_{12} &= \frac{1}{\sqrt{2}}a_1 v_s + \frac{1}{2}v_1 v_2\lambda_4 + \mu_3^2, \\ \left[M^2_{\pm}\right]_{22} &= v_2^2\lambda_2 + \frac{1}{2}\left(v_s^2\lambda_3' + v_1^2\lambda_3 - \frac{1}{v_2}\left[a_1 v_1 v_s\sqrt{2} + 2v_2^3\lambda_2 + v_2 v_s^2\lambda_2' + v_1^2 v_2\lambda_3 + v_1^2 v_2\lambda_4 + 2v_1\mu_3^2\right]\right). \end{aligned} \tag{A.6}$$

Upon rotation to the Higgs basis, the CP-even mass matrix becomes:

$$M^2_{0,H,\text{even}} = \begin{pmatrix} \left[M^2_{0,H,\text{even}}\right]_{11} & \left[M^2_{0,H,\text{even}}\right]_{12} & \left[M^2_{0,H,\text{even}}\right]_{13} \\ \left[M^2_{0,H,\text{even}}\right]_{12} & \left[M^2_{0,H,\text{even}}\right]_{22} & \left[M^2_{0,H,\text{even}}\right]_{23} \\ \left[M^2_{0,H,\text{even}}\right]_{13} & \left[M^2_{0,H,\text{even}}\right]_{23} & \left[M^2_{0,H,\text{even}}\right]_{33} \end{pmatrix}, \tag{A.7}$$

where the elements are:

$$\begin{aligned} \left[M^2_{0,H,\text{even}}\right]_{11} &= \frac{2}{v^2}\left(v_1^4\lambda_1 + v_2^4\lambda_2 + v_1^2 v_2^2\left[\lambda_3 + \lambda_4\right]\right), \\ \left[M^2_{0,H,\text{even}}\right]_{12} &= \frac{v_1 v_2}{v^2}\left(2v_2^2\lambda_2 - v_2^2\left[\lambda_3 + \lambda_4\right] + v_1^2\left[\lambda_3 + \lambda_4 - 2\lambda_1\right]\right), \\ \left[M^2_{0,H,\text{even}}\right]_{13} &= \frac{1}{v}\left(a_1 v_1 v_2\sqrt{2} + v_1^2 v_s\lambda_2' + v_2^2 v_s\lambda_3'\right), \\ \left[M^2_{0,H,\text{even}}\right]_{22} &= 2v_1^2\left(\lambda_1 + \lambda_2 - \lambda_3 - \lambda_4\right) + \frac{2v_1^4}{v^2}\left(\lambda_3 + \lambda_4 - \lambda_1 - \lambda_2\right) - \frac{v_1}{v_2}\left(a_1 v_s\sqrt{2} + 2\mu_3^2\right) + \\ &- \frac{v_2}{v_1}\left(a_1 v_s\sqrt{2} + 2\mu_3^2\right), \\ \left[M^2_{0,H\text{even}}\right]_{23} &= \frac{1}{2v}\left(a_1\left[v_1^2 - v_2^2\right]\sqrt{2} + 2v_1 v_2 v_s\left[\lambda_3' - \lambda_2'\right]\right), \\ \left[M^2_{0,H\text{even}}\right]_{33} &= 2v_s^2\lambda_1' - \frac{1}{v_s\sqrt{2}}a_1 v_1 v_2. \end{aligned} \tag{A.8}$$

The CP-odd mass matrix in the Higgs basis:

$$M^2_{0,H,\text{even}} = \begin{pmatrix} 0 & 0 & 0 \\ 0 & \left[M^2_{0,H,\text{odd}}\right]_{22} & \left[M^2_{0,H,\text{odd}}\right]_{23} \\ 0 & \left[M^2_{0,H,\text{odd}}\right]_{23} & \left[M^2_{0,H,\text{odd}}\right]_{33} \end{pmatrix}, \tag{A.9}$$

where the elements are:

$$\begin{aligned} \left[M^2_{0,\text{odd}}\right]_{22} &= -\frac{v^2}{2v_1v_2}\left(a_1 v_s\sqrt{2} + 2\mu_3^2\right), \\ \left[M^2_{0,\text{odd}}\right]_{23} &= -\frac{1}{\sqrt{2}}a_1 v, \\ \left[M^2_{0,\text{odd}}\right]_{33} &= -\frac{1}{2v_s}\left(a_1 v_1 v_2\sqrt{2} + 4v_s\mu_b^2\right). \end{aligned} \tag{A.10}$$

As stated earlier, the charged scalar mass matrix in the Higgs basis is diagonal in our model:

$$M^2_{\pm,H} = \begin{pmatrix} 0 & 0 \\ 0 & -\frac{v^2}{2v_1v_2}\left(a_1 v_s\sqrt{2} + v_1v_2\lambda_4 + 2\mu_3^2\right) \end{pmatrix}. \tag{A.11}$$

B Inverted Parameters

Here, we present a selection of the parameters of the scalar expressed in terms of masses and mixing angles. For brevity, we use the shorthand notation: $\cos\alpha_1 = c_{\alpha_1}$.

$$a_1 = \frac{1}{v}\left(\cos\gamma_1 \sin\gamma_1 \left[m_\chi^2 - m_A^2\right]\sqrt{2}\right), \tag{B.12}$$

$$\mu_b^2 = -\frac{1}{2}\left(m_A^2\cos^2(\gamma_1) + m_\chi^2\sin^2(\gamma_1) + \frac{a_1 v_1 v_2}{\sqrt{2}v_s}\right), \tag{B.13}$$

$$\mu_3^2 = -\frac{1}{2v^2}\left(m_A^2 v_1 v_2\cos^2(\gamma_1) + m_\chi^2 v_1 v_2\sin^2(\gamma_1)\right) - \frac{a_1 v_s}{\sqrt{2}}, \tag{B.14}$$

$$\begin{aligned} \lambda_1 = \frac{1}{4v^2v_1^3}\Big(&v^2 v_2\left[a_1 v_s\sqrt{2} + 2\mu_3^2\right] + 2m_h^2 v_1 c_{\alpha_2}^2\left[v_1 c_{\alpha_3} - v_2 s_{\alpha_3}\right]^2 + \\ &- 4v_1 c_{\alpha_1}s_{\alpha_1}s_{\alpha_2}\left[m_H^2 - m_\varsigma^2\right]\left[v_1 v_2 c_{2\alpha_3} + \left(v_1^2 - v_2^2\right)c_{\alpha_3}s_{\alpha_3}\right] + \\ &+ 2v_1 s_{\alpha_1}^2\left[c_{\alpha_3}^2\left(m_\varsigma^2 v_2^2 + m_H^2 v_1^2 s_{\alpha_2}^2\right) + s_{\alpha_3}^2\left(m_\varsigma^2 v_1^2 + m_H^2 v_s^2 s_{\alpha_2}^2\right) + v_1 v_2 s_{2\alpha_3}\left(m_\varsigma^2 - m_H^2 s_{\alpha_2}^2\right)\right] + \\ &+ 2v_1 c_{\alpha_1}^2\left[c_{\alpha_3}^2\left(m_H^2 v_2^2 + m_\varsigma^2 v_1^2 s_{\alpha_2}^2\right) + s_{\alpha_3}^2\left(m_H^2 v_1^2 + m_\varsigma^2 v_s^2 s_{\alpha_2}^2\right) + v_1 v_2 s_{2\alpha_3}\left(m_H^2 - m_\varsigma^2 s_{\alpha_2}^2\right)\right]\Big), \end{aligned} \tag{B.15}$$

$$\begin{aligned} \lambda_2 = \frac{1}{8v_1v_2^3}\Big(&2v^2\left[a_1 v_s\sqrt{2} + 2\mu_3^2\right] + v_1 v_2\left[2m_h^2 + 3\left(m_H^2 + m_\varsigma^2\right) - 8v_1^2\lambda_1 + \right. \\ &\left. + 2c_{2\alpha_1}c_{\alpha_2}^2\left(m_H^2 - m_\varsigma^2\right)c_{2\alpha_2}\left(2m_h^2 - m_H^2 - m_\varsigma^2\right)\right]\Big), \end{aligned} \tag{B.16}$$

$$\begin{aligned} \lambda_3 = \frac{1}{2v_1^2v_2^2}\Big(&v^2\left[c_{\alpha_3}^2\left(m_h^2 c_{\alpha_2}^2 + s_{\alpha_2}^2\left[m_H^2 s_{\alpha_1}^2 + m_\varsigma^2 c_{\alpha_1}^2\right]\right) + 2c_{\alpha_1}c_{\alpha_3}s_{\alpha_1}s_{\alpha_2}s_{\alpha_3}\left(m_\varsigma^2 - m_H^2\right) + \right. \\ &\left. + s_{\alpha_3}^2\left(m_H^2 c_{\alpha_1}^2 + m_\varsigma^2 s_{\alpha_1}\right)\right] - 2\left[v_1^4\lambda_1 + v_2^4\lambda_2 + v_1^2 v_2^2\lambda_4\right]\Big), \end{aligned} \tag{B.17}$$

$$\lambda_4 = -\frac{\sqrt{2}a_1 v_s + 2\mu_3^2}{v_1 v_2} - \frac{2m_{H^\pm}^2}{v^2}, \tag{B.18}$$

$$\lambda_1' = \frac{1}{4v_s^3}\left(a_1 v_1 v_2\sqrt{2} + 2v_s\left[c_{\alpha_2}^2\left(m_H^2 s_{\alpha_1}^2 + m_\varsigma^2 c_{\alpha_1}^2\right) + m_h^2 s_{\alpha_2}^2\right]\right), \tag{B.19}$$

$$\begin{aligned}\lambda_2' = \frac{1}{2vv_1v_s}\Big(&a_1 v_2 v^2\sqrt{2} + \left[m_H^2 - m_\varsigma^2\right] v c_{\alpha_2} s_{2\alpha_1}\left[v_2 c_{\alpha_3} + v_1 s_{\alpha_3}\right] + \\ &+\frac{1}{2}v\left[2m_h^2 - m_H^2 - m_\varsigma^2 + \left(m_H^2 - m_\varsigma^2\right)c_{2\alpha_1}\right] s_{2\alpha_2}\left[v_1 c_{\alpha_3} - v_2 s_{\alpha_3}\right]\Big),\end{aligned} \tag{B.20}$$

$$\begin{aligned}\lambda_3' = \frac{1}{2v_1v_2v_s}\Big(&a_1\left[v_2^2 - v_1^2\right]\sqrt{2} + 2v_1 v_2 v_s\lambda_2' + 2vc_{\alpha_2}\left[\left(m_H^2 - m_\varsigma^2\right)c_{\alpha_1}c_{\alpha_3}s_{\alpha_1} + \right. \\ &+ \left.\left(m_H^2 s_{\alpha_1}^2 + m_\varsigma^2 c_{\alpha_1}^2 - m_h^2\right) s_{\alpha_2}s_{\alpha_3}\right]\Big).\end{aligned} \tag{B.21}$$

C Software Manual

In this section we describe how to use the software BGLNCSexplorer that can be found at [10] (there the up-to-date version of the program and manual can be found). The repository contains the SARAH models used, the corresponding SPheno set-up codes, bash scripts for running the codes on a cluster and finally the Python files that constitute the actual program.

The software is divided into two, separately executed, chains of scripts. The first one is started from `wrapper_master.py` and performs the scan. The scan is configured from the plain text file `config_file` where the user can specify the number of points to be created, the ranges over which to scan all the free parameters (assumed to be in GeV wherever applicable), the versions of the external software that are installed (SARAH, SPheno, HiggsBounds and HiggsSignals) and what data is to be saved.

Once the first chain has been run at least once, generating some data, the other chain may be executed. This chain loads the saved data and analyzes it, producing plots depicting the data and the results of the analysis. It is started by running `analysis_and_plotting.py` and can be configured from the plain text file `analysis_config_file`. In the configuration file, the user can specify which (implemented) flavor observables to plot. The experimental data corresponding to those flavor observables can also be specified here (required to plot 1 σ C.L. limits). In addition a switch exists in the configuration file that allows for the creation of a register that stores the location of all the points that had passed all bounds (up to and including HiggsBounds and HiggsSignals). The usage of such a register allows for a faster subsequent runs of the `analysis_and_plotting.py` chain of codes.

All the files comprising the two chains are summarized in table 4. In addition, a set of bash scripts for running the codes in a HPC environment (configured for LUNARC Aurora cluster) can be found in the repository. They are written to work together with the aforementioned Python chains with minimal intervention from the user. A summary of them can be found in table 5.

Table 4: *The function and interdependence of the* PYTHON *files that make up the* BGLNCSEXPLORER.

PYTHON File	Description	Dependence
`wrapper_master.py`	**The main execution file**.	Calls `wrapper_loop.py` and `data_handling,py`
`wrapper_loop.py`	The main loop. 1 Iteration = 1 Point.	Calls `inversion_procedure.py`, `electroweak_precision_observables.py` and `file_writing.py`
`analysis_and_plotting.py`	Harvests from files and analyzes the data. **Executed independently from master**.	Calls `visualization.py` and `file_writing.py`
`inversion_procedure.py`	Implements the inversion procedure for the Yukawa and scalar sectors.	None
`electroweak_precision_observables.py`	Calculates the electroweak precision observables.	None
`file_writing.py`	Saves the preSPheno data, writes the SLHA input file for SPHENO.	None
`data_handling.py`	Bunches the data into larger files, tosses out unneeded data.	None
`visualization.py`	Creates the plots.	None

Table 5: *The function and interdependence of the* BASH *scripts that allow for running in a hpc environment.*

BASH File	Description	Dependence
`master.sh`	The execution file of the `wrapper_master.py` chain of codes. Parallerizes the simulation process over processor cores.	Calls `workScript.sh` for each parallel process
`workScript.sh`	Runs the `wrapper_master.py` chain of codes. Called for each processor core by `master.sh`	None
`analysis_submit.sh`	Analyzes the previously collected and stored data. Uses the `analysis_and_plotting.py` chain of codes.	None

References

[1] ATLAS collaboration, *Observation of a new particle in the search for the Standard Model Higgs boson with the ATLAS detector at the LHC*, *Phys. Lett. B* **716** (2012) 1 [1207.7214].

[2] CMS collaboration, *Observation of a new boson at a mass of 125 GeV with the CMS experiment at the LHC*, *Phys. Lett. B* **716** (2012) 30 [1207.7235].

[3] I.P. Ivanov, *Building and testing models with extended Higgs sectors*, *Progress in Particle and Nuclear Physics* **95** (2017) 160 .

[4] T. Lee, *CP nonconservation and spontaneous symmetry breaking*, *Physics Reports* **9** (1974) 143 .

[5] S.L. Glashow and S. Weinberg, *Natural conservation laws for neutral currents*, *Phys. Rev. D* **15** (1977) 1958.

[6] E.A. Paschos, *Diagonal neutral currents*, *Phys. Rev. D* **15** (1977) 1966.

[7] G. Branco, P. Ferreira, L. Lavoura, M. Rebelo, M. Sher and J.P. Silva, *Theory and phenomenology of two-Higgs-doublet models*, *Physics Reports* **516** (2012) .

[8] A.D. Sakharov, *SPECIAL ISSUE: violation of CP invariance, C asymmetry, and baryon asymmetry of the universe*, *Soviet Physics Uspekhi* **34** (1991) 392.

[9] A. Ordell, *Phenomenology in multi-scalar extensions of the Standard Model*, Ph.D. thesis, Lund University, 2020.

[10] M. Nowak, "*BGLNCSexplorer*." `github.com/MichalNowak0/BGLNCSexplorer`, 2021.

[11] G. Branco, W. Grimus and L. Lavoura, *Relating the scalar flavour-changing neutral couplings to the CKM matrix*, *Physics Letters B* **380** (1996) 119 .

[12] M. Blanke, *Introduction to flavour physics and CP violation*, 2017.

[13] G. Kane, *Modern elementary particle physics: explaining and extending the Standard Model*, Cambridge University Press, 2 ed. (2017).

[14] M.E. Peskin and D.V. Schroeder, *An introduction to quantum field theory*, Addison-Wesley, Reading, USA (1995).

[15] S.L. Glashow, J. Iliopoulos and L. Maiani, *Weak interactions with lepton-hadron symmetry*, *Phys. Rev. D* **2** (1970) 1285.

[16] J.P. Ellis, *TikZ-Feynman: feynman diagrams with TikZ*, *Computer Physics Communications* **210** (2017) 103.

[17] T.D. Lee, *A theory of spontaneous T violation*, *Phys. Rev. D* **8** (1973) 1226.

[18] B.W. Lee, C. Quigg and H.B. Thacker, *Weak interactions at very high energies: the role of the Higgs-boson mass*, *Phys. Rev. D* **16** (1977) 1519.

[19] D. Das and I. Saha, *Alignment limit in three Higgs-doublet models*, *Phys. Rev. D* **100** (2019) .

[20] L. Siwe, *Using neural networks to probe the parameter space of a 3HDM with a $U(1) \times Z_2$ flavor symmetry*, Master's thesis, Lund University, 2020.

[21] I. Padilla, *Phenomenology of a three Higgs doublet model with a $U(1) \times Z_2$ flavour symmetry*, Master's thesis, Lund University, 2019.

[22] A. Ordell, R. Pasechnik and H. Serôdio, *Anomaly-free 2HDMs with a gauged Abelian symmetry and two generations of right-handed neutrinos*, *Phys. Rev. D* **102** (2020) .

[23] F. Nottensteiner, A. Ordell, R. Pasechnik and H. Serôdio, *Classification of anomaly-free 2HDMs with a gauged $U(1)^{'}$ symmetry*, *Phys. Rev. D* **100** (2019) .

[24] A. Rasin, *Diagonalization of quark mass matrices and the Cabibbo-Kobayashi-Maskawa matrix*, `hep-ph/9708216`.

[25] Particle Data Group collaboration, *Review of particle physics*, *PTEP* **2020** (2020) .

[26] L. Wolfenstein, *Parametrization of the Kobayashi-Maskawa matrix*, *Phys. Rev. Lett.* **51** (1983) 1945.

[27] C. Jarlskog, *Commutator of the quark mass matrices in the Standard Electroweak Model and a measure of maximal* CP *nonconservation*, *Phys. Rev. Lett.* **55** (1985) 1039.

[28] K. Kannike, *Vacuum stability conditions from copositivity criteria*, *Eur. Phys. J. C* **72** (2012) .

[29] B.W. Lee, C. Quigg and H.B. Thacker, *Strength of weak interactions at very high energies and the Higgs boson mass*, *Phys. Rev. Lett.* **38** (1977) 883.

[30] S. Moretti and K. Yagyu, *Constraints on parameter space from perturbative unitarity in models with three scalar doublets*, *Phys. Rev. D* **91** (2015) .

[31] R. Coimbra, M. Sampaio and R. Santos, *SCANNERS: constraining the phase diagram of a complex scalar singlet at the LHC*, *Eur. Phys. J. C* **73** (2013) .

[32] M. Bento, H. Haber, J. Romao and J. Silva, *Multi-Higgs doublet models: physical parametrization, sum rules and unitarity bounds*, *J. High Energ. Phys.* **95** (2017) .

[33] W. Grimus, L. Lavoura, O. Ogreid and P. Osland, *The oblique parameters in multi-Higgs-doublet models*, *Nuclear Physics B* **801** (2008) 81.

[34] P. Bechtle, O. Brein, S. Heinemeyer, G. Weiglein and K. Williams, *HiggsBounds: confronting arbitrary Higgs sectors with exclusion bounds from LEP and the Tevatron*, *Computer Physics Communications* **181** (2010) 138.

[35] P. Bechtle, O. Brein, S. Heinemeyer, G. Weiglein and K. Williams, *HiggsBounds 2.0.0: confronting neutral and charged Higgs sector predictions with exclusion bounds from LEP and the Tevatron*, *Computer Physics Communications* **182** (2011) 2605.

[36] P. Bechtle, O. Brein, S. Heinemeyer, O. Stål, T. Stefaniak, G. Weiglein et al., *Recent developments in HiggsBounds and a preview of HiggsSignals*, 2013.

[37] P. Bechtle, O. Brein, S. Heinemeyer, O. Stål, T. Stefaniak, G. Weiglein et al., *HiggsBounds-4: improved tests of extended Higgs sectors against exclusion bounds from LEP, the Tevatron and the LHC*, *Eur. Phys. J. C* **74** (2014) .

[38] P. Bechtle, S. Heinemeyer, O. Stål, T. Stefaniak and G. Weiglein, *Applying exclusion likelihoods from LHC searches to extended Higgs sectors*, *Eur. Phys. J. C* **75** (2015) .

[39] W. Porod, *SPheno, a program for calculating supersymmetric spectra, SUSY particle decays and SUSY particle production at e+e- colliders*, *Computer Physics Communications* **153** (2003) 275 .

[40] W. Porod and F. Staub, *SPheno 3.1: extensions including flavour, CP-phases and models beyond the MSSM*, *Computer Physics Communications* **183** (2012) 2458 .

[41] P. Bechtle, S. Heinemeyer, O. Stål, T. Stefaniak and G. Weiglein, *HiggsSignals: confronting arbitrary Higgs sectors with measurements at the Tevatron and the LHC*, *Eur. Phys. J. C* **74** (2014) .

[42] F. Staub, *SARAH 4: a tool for (not only SUSY) model builders*, *Computer Physics Communications* **185** (2014) 1773 .

[43] W. Porod, F. Staub and A. Vicente, *A flavor kit for BSM models*, *Eur. Phys. J. C* **74** (2014) .

[44] D.M. Straub, *flavio: a Python package for flavour and precision phenomenology in the Standard Model and beyond*, 2018.